Aquatic environment drives the emergence of cell wall-deficient dormant forms in Listeria

Filipe Carvalho, Alexis Carreaux, Anna Sartori-Rupp, Stéphane Tachon, Anastasia D Gazi, Pascal Courtin, Pierre Nicolas, Florence Dubois-Brissonnet, Aurélien Barbotin, Emma Desgranges, et al.

nature communications

Article

https://doi.org/10.1038/s41467-024-52633-7

Aquatic environment drives the emergence of cell wall-deficient dormant forms in *Listeria*

Received: 21 November 2023

Accepted: 16 September 2024

Published online: 02 October 2024

Check for updates

Filipe Carvalho[1], Alexis Carreaux[1], Anna Sartori-Rupp[2], Stéphane Tachon[2], Anastasia D. Gazi[3], Pascal Courtin[1], Pierre Nicolas[4], Florence Dubois-Brissonnet[1], Aurélien Barbotin[1], Emma Desgranges[1], Matthieu Bertrand[1], Karine Gloux[1], Catherine Schouler[5], Rut Carballido-López[1], Marie-Pierre Chapot-Chartier[1], Eliane Milohanic[1], Hélène Bierne[1] & Alessandro Pagliuso[1]

Stressed bacteria can enter a dormant viable but non-culturable (VBNC) state. VBNC pathogens pose an increased health risk as they are undetectable by growth-based techniques and can wake up back into a virulent state. Although widespread in bacteria, the mechanisms governing this phenotypic switch remain elusive. Here, we investigate the VBNC state transition in the human pathogen *Listeria monocytogenes*. We show that bacteria starved in mineral water become VBNC by converting into osmotically stable cell wall-deficient coccoid forms, a phenomenon that occurs in other *Listeria* species. We reveal the bacterial stress response regulator SigB and the autolysin NamA as major actors of VBNC state transition. We lastly show that VBNC *Listeria* revert to a walled and virulent state after passage in chicken embryos. Our study provides more detail on the VBNC state transition mechanisms, revealing wall-free bacteria naturally arising in aquatic environments as a potential survival strategy in hypoosmotic and oligotrophic conditions.

Bacteria often face less than optimal growth conditions and a variety of abiotic stresses in their environment. Some species are able to produce highly resistant cellular structures, called endospores, to enter a metabolically inactive state until environmental conditions are adequate for resuming vegetative growth[1]. Alternatively, bacteria may enter a dormant state known as the viable but non-culturable (VBNC) state, in which they preserve some metabolic activity at the expense of losing the ability to grow on regular culture media[2]. The VBNC state is documented in over a hundred species[2,3], but our knowledge concerning the molecular processes driving the transition from a vegetative lifestyle to the VBNC state, particularly in Gram-positive bacteria, are still fragmentary.

The transition to a VBNC state is frequently accompanied by a morphological change, often cell dwarfing and/or rounding[4]. The underlying reasons are not entirely understood but an hypothesis is that a spherical shape, with a smaller surface area/volume ratio, might help VBNC bacteria reduce their energy demands and optimize nutrient uptake[5]. Studies mostly performed in Gram-negative bacteria reported structural modifications of the cell wall (CW) peptidoglycan recovered from VBNC cells that might contribute to cell rounding[6–8]. However, a direct link between CW modifications, cell morphology and dormancy has not yet been clearly established.

Cell rounding has also been observed when some bacteria switch into a CW-deficient (CWD) state. This is the case of L-forms, CWD variants generated by exposure to CW-targeting agents, such as wall-active antibiotics, lytic enzymes or phages[9–11]. L-form cells remain viable and able to replicate, but the absence of CW makes them sensitive to

[1]INRAE, Université Paris-Saclay, AgroParisTech, Micalis Institute, Jouy-en-Josas, France. [2]NanoImaging Core Facility, Institut Pasteur, Paris, France. [3]Ultrastructural Bioimaging Facility, Institut Pasteur, Paris, France. [4]INRAE, Université Paris-Saclay, MaIAGE, Jouy-en-Josas, France. [5]INRAE, Université de Tours, ISP, Nouzilly, France. e-mail: alessandro.pagliuso@inrae.fr

osmotic lysis, and therefore they need to be cultivated in osmoprotective conditions[9]. For this reason, the physiological relevance of L-forms, and CWD bacteria in general, is a matter of debate[9].

Here, we report that the Gram-positive bacterium *Listeria monocytogenes* (*Lm*) undergoes a rod-to-coccus differentiation during transition to a VBNC state in a nutrient-deprived natural water setting. We reveal that this cell rounding results from loss of the CW via a molting-like shedding process. These CWD VBNC *Lm* forms are resistant to osmotic lysis, likely as a result of adaptive changes in the physicochemical properties of their plasma membrane. To our knowledge, this is the first report of CWD VBNC bacteria naturally arising in a non-osmotically stabilized environment. We identify the stress-responsive transcription factor SigB and the autolysin NamA as major molecular players in the formation of CWD VBNC *Lm*. We further show that this CWD VBNC state is extensive to other *Listeria sensu stricto* species. Finally, we show that dormant wall-less *Lm* can revert back to a walled, vegetative and fully virulent state after passage in embryonated chicken eggs. Our results suggest that CW shedding is an adaptive process employed by *Listeria* to survive under prolonged nutritional limitation.

Results

Dynamics of VBNC *Lm* formation in mineral water

To induce a VBNC state in *Lm*, we followed a starvation-based approach by incubating *Lm* in water[12,13]. We used the EGDe strain as our reference wild-type *Lm* strain, and a commercial mineral water as our starvation medium due to its natural spring origin, low mineral content and quality-controlled composition (Supplementary Table 1). As the starting number of bacteria affects the dynamics of culturability loss[13], we tested initial *Lm* concentrations ranging from 10^9 to 10^6 bacteria/mL. We observed that the rate and magnitude of culturability loss increased when the starting bacterial concentration was reduced (Fig. 1a). Notably, a concentration of 10^6 *Lm*/mL resulted in culturability levels of <1 colony-forming units (CFU)/mL after 28 days (Fig. 1a). We chose a starting concentration of 10^8 *Lm*/mL as the standard condition to induce the VBNC state in mineral water throughout this work, since it produces a 2-log drop in culturable *Lm* after 28 days while still providing sufficient material for downstream analyzes.

To confirm the formation of VBNC *Lm*, we monitored the total number of bacteria and the fraction of viable bacteria by flow cytometry at each time point. The viable population was determined using carboxyfluorescein diacetate (CFDA, Supplementary Fig. 1a), a fluorogenic dye that is enzymatically activated and retained in the cytoplasm of metabolically active bacteria with an integral plasma membrane[14]. While CFU counts dropped progressively to 10^6 *Lm*/mL after 28 days, the total and viable population numbers remained nearly unchanged (Fig. 1b). The increasing difference between the viable and culturable populations with time demonstrates the gradual and almost complete transition to a VBNC state (Fig. 1c). This was also observed when using the double-dye Live/Dead assay to assess plasma membrane permeability to cell-impermeable probes as a readout of cell viability (Supplementary Fig. 1b). In this case, viable population numbers drop more with time in comparison with the CFDA assay. This can be partly explained by the fact that viable cells can have temporarily leaky membranes, in response to certain conditions, which results in their mislabeling as dead and underestimation of the viable population[15].

ATP is only produced by live cells and quickly depleted upon cell death, constituting thus a marker of cellular viability. In cases of bacterial dormancy, such as persister or VBNC cells, a reduced metabolic state is associated with a residual ATP content[3]. We measured the intracellular ATP levels in mineral water-incubated *Lm* cells over time, in parallel to their culturability. Variations in the ATP content did not follow the changes in culturability, unlike what we observed from a dilution series of freshly prepared suspensions, used to report the ATP content expected from a given number of culturable cells (Fig. 1d). Indeed, whereas culturable *Lm* numbers declined steadily, ATP levels dropped drastically after 7 days, recovering partially afterwards. Importantly, from day 21, the measured ATP levels were higher than those expected from a similar number of culturable cells (Fig. 1d), suggesting that this ATP surplus comes from the larger, non-culturable *Lm* subpopulation.

Together, these results confirm the transition of *Lm* to a VBNC state in mineral water.

VBNC *Lm* assume a coccoid morphology in mineral water

Changes in the bacterial cell size and shape are frequently associated with the VBNC state[4]. We thus acquired phase-contrast images of *Lm* EGDe suspensions in mineral water to track the occurrence of morphological changes during VBNC cell formation. The initial *Lm* population (day 0) consisted of typical rod-shaped cells, isolated or in tethered pairs (Fig. 1e). From 7 days of incubation, coccoid forms were also observed and became more abundant over time, at the expense of the rod-shaped subpopulation (Fig. 1e). Quantitative analysis of the populational morphology confirmed this progressive rod-to-coccus shape transformation (Fig. 1f, g). A suspension of GFP-expressing *Lm* showed GFP-positive coccoid cells appearing as of day 7 and increasing in number by day 28 (Supplementary Fig. 2), further confirming that the spherical forms derive from the initial rod-shaped *Lm*. Noteworthy, coccoid cells were sometimes found next to phase-light rod-shaped structures resembling empty cell wall sacculi (Fig. 1e, insets day 14 and 21).

These results show that incubation in mineral water triggers a rod-to-coccus transition in *Lm* cells. Interestingly, the dynamics of this morphological transition closely overlap with the dynamics of culturability decline and VBNC cell formation (Fig. 1b, c), suggesting a link between the shape change and the transition to a VBNC state.

Rod-to-coccus change is caused by a molting-like CW loss event

The switch from rod to coccoid shape has been observed in bacteria converting to L-forms, with the loss of the CW as the main driving force of this morphological change[9,16,17]. Having observed coccoid *Lm* associated with ghost structures resembling empty cell wall sacculi (Fig. 1e), we investigated whether coccoid *Lm* cells were CWD forms. We first performed a Gram staining of the *Lm* EGDe population at day 0 and day 28. Remarkably, the usual crystal violet staining displayed by rod-shaped *Lm* cells at day 0 was no longer present when the population consisted of coccoid cells after 28 days in mineral water (Fig. 1h), indicating the absence of a typical Gram-positive CW in coccoid VBNC *Lm* cells. We then compared the peptidoglycan content purified from equivalent *Lm* cell numbers at different timepoints of incubation in water, by performing UHPLC analysis of muropeptides. The muropeptide elution profiles showed that, while their composition did not visibly change, the amount of the different muropeptide species decreased with time until virtually no peptidoglycan was detected by day 28 (Fig. 1i). Together, these results confirm the progressive depletion of the *Lm* CW during transition to a VBNC state.

Next, we monitored the dynamics of *Lm* CW loss by fluorescence microscopy. The walled *Lm* population was fluorescently stained with wheat germ agglutinin (WGA), a lectin that binds to free *N*-acetylglucosamine (GlcNAc) residues present in wall teichoic acids (WTAs) of serogroup 1/2 strains[18]. To monitor in parallel the appearance of CWD *Lm* cells, we generated anti-CWD *Lm* antibodies after immunization of rabbits with CWD *Lm* recovered from mineral water suspensions after 28 days. The anti-CWD *Lm* antibodies labeled the coccoid (i.e. CWD) but not the rod-shaped (i.e. walled) *Lm* cells, confirming their specificity (Supplementary Fig. 3). On the first day, *Lm* cells were only stained by WGA, indicating intact CW and a plasma membrane externally inaccessible to labeling by the anti-CWD *Lm* (Fig. 1j, k). Two additional subpopulations emerged with time: double-labeled cells, corresponding to *Lm* with a more permeable/damaged CW, and cells labeled only by the anti-CWD *Lm*, representing CWD *Lm* (Fig. 1j, k). The fraction of CWD *Lm* progressively increased with time to represent >95% of bacteria by day 28 (Fig. 1k).

https://doi.org/10.1038/s41467-024-52633-7

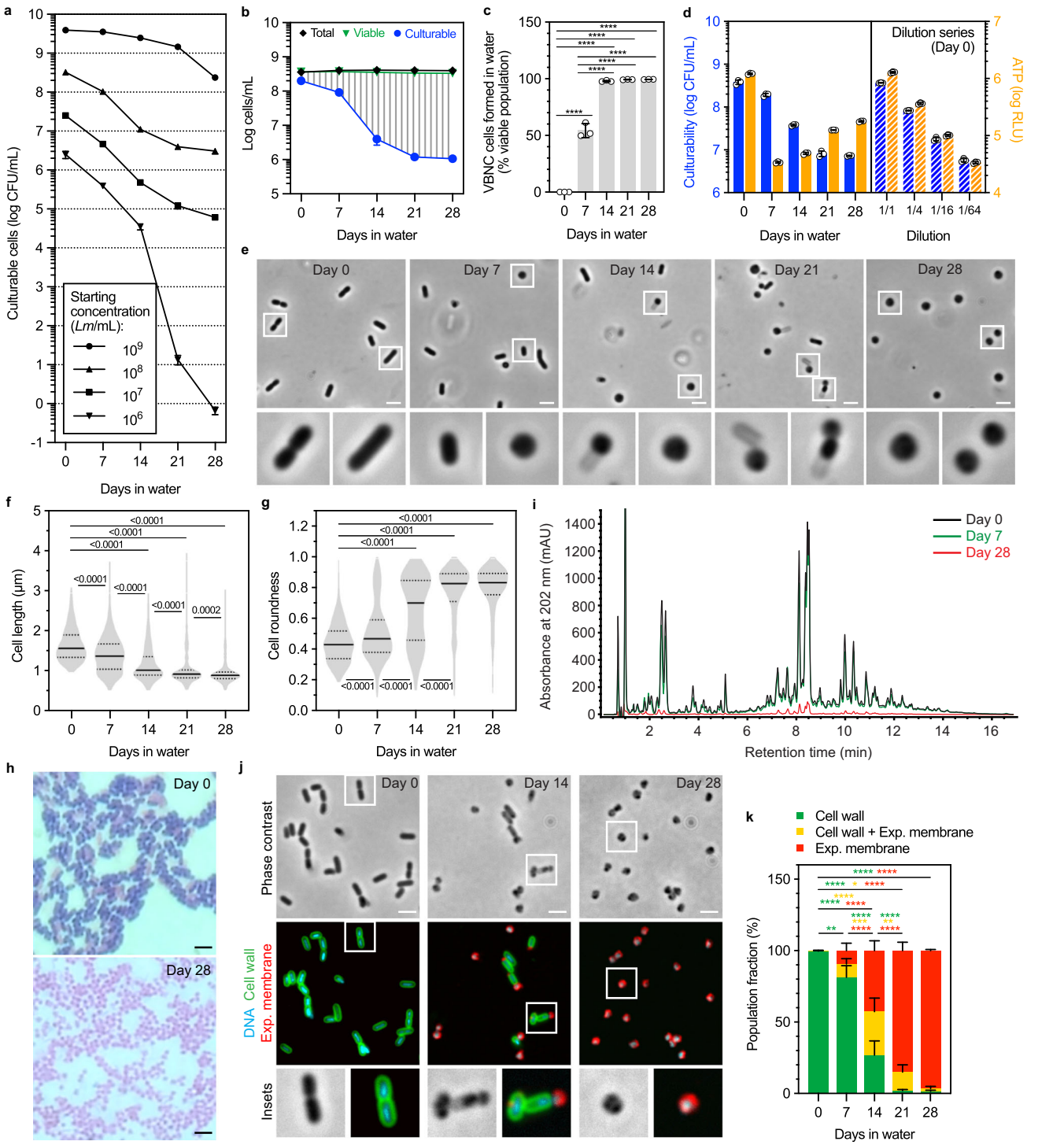

Fig. 1 | *Lm* transitions into a CWD VBNC state during incubation in mineral water. a Culturability of *Lm* EGDe in mineral water with different starting bacterial concentrations. Culturable bacteria were quantified by colony-forming unit (CFU) enumeration. **b** Total, viable, and culturable cell numbers of *Lm* EGDe in mineral water. Culturable bacteria (blue circles) were quantified as in **a**; total (black diamonds) and viable (green triangles) bacteria were quantified by flow cytometry using CFDA. Dashed area indicates VBNC population. **c** Fraction of the viable population shown in **b** consisting of VBNC cells formed in mineral water. **d** Culturability vs. ATP content of *Lm* EGDe in mineral water. Culturable bacteria (blue bars) were quantified as in **a**; ATP (orange bars) was quantified with a luciferase-based assay. Dashed bar graph shows results for a dilution series of *Lm* EGDe in mineral water (day 0) as a reference for the ATP levels expected from a defined number of culturable cells. **e** Phase-contrast micrographs of *Lm* EGDe in mineral water. Bacteria highlighted in white squares are shown enlarged in bottom panels. **f, g** Cell length and roundness of *Lm* EGDe in mineral water. **h** Brightfield micrographs of Gram-stained *Lm* EGDe sampled from mineral water. **i** Peptidoglycan muropeptide profiles of *Lm* EGDe sampled from mineral water at indicated time points. **j** Phase-contrast and fluorescence micrographs of *Lm* EGDe fluorescently labeled for DNA (cyan), cell wall (green), and exposed plasma membrane (red). Bacteria highlighted in white squares are shown enlarged in bottom panels. **k** Fraction of the *Lm* EGDe population showing single- or double-labeling of cell wall and exposed plasma membrane by fluorescence microscopy. Data are expressed as mean ± standard deviation (**a**–**d**, **k**) or median + interquartile range (**f**, **g**) of three independently prepared bacterial suspensions, or are representative of two independently prepared suspensions (**h, i**). Statistical significance was determined with one-way ANOVA with Tukey's test (**c**), Kruskal-Wallis test with Dunn's post hoc test (**f**, **g**), or two-way ANOVA with Tukey's test (**k**). *$p \le 0.05$; **$p \le 0.01$; ***$p \le 0.001$; ****$p \le 0.0001$. Scale bars: 2 µm. Source data are provided as a Source Data file.

Lastly, we investigated the CW loss phenomenon at the ultrastructural level in near-native conditions by cryogenic electron tomography (cryo-ET) of whole *Lm* EGDe cells. Micrographs and 3D rendering of segmented tomograms acquired at day 0 and 14 allowed us to reconstruct the different stages of the morphological transition of *Lm* in mineral water. Starting as a rod-shaped bacterium with a CW wrapped tightly around the plasma membrane (Fig. 2, stage 0; Supplementary Movie 1), *Lm* starts showing a substantial detachment between these two layers (Fig. 2, stage 1), followed by the weakening and appearance of variably sized gaps in the CW mesh (Fig. 2, stage 2; Supplementary Movie 2). These gaps allow the enclosed protoplast to gradually egress the CW sacculus (Fig. 2, stages 3 and 4; Supplementary Movies 3 and 4) and escape into the extracellular medium as a spherical cell (Fig. 2, stage 5; Supplementary Movie 5).

Altogether, these results reveal that *Lm* cells transitioning to a VBNC state lose their CW through a molting-like shedding process that generates wall-less coccoid cell forms.

A CWD VBNC state is widespread in *Listeria* species

We next wondered if the CWD VBNC state induced in mineral water occurred in other *Lm* strains, besides our reference strain EGDe. We monitored VBNC cell formation in the *Lm* strain 10403S, another well-studied reference laboratory strain[19], and in two clinical *Lm* strains isolated from human and bovine listeriosis cases: CLIP 63713 and JF5203, respectively[20,21]. Similar to EGDe, these three strains showed declining culturability over time (Supplementary Fig. 4a–d) and formation of a VBNC subpopulation (Supplementary Fig. 4e–h) in mineral water. To monitor the presence of CW by fluorescence microscopy, we used a commercial antibody raised against *Lm* CW-specific antigens (anti-*Lm*), since WGA does not label the CW of *Lm* serogroup 4 strains (CLIP 63713 and JF5203) due to the lack of free GlcNAc residues in their WTAs[22,23]. The three strains displayed gradual loss of the CW (Supplementary Fig. 4i–l, q) and exposure of the plasma membrane (Supplementary Fig. 4m–p, q), with dynamics comparable to those of VBNC cell formation. These results demonstrate that the formation of CWD VBNC forms is a strain-independent property of *Lm*.

We then investigated other *Listeria* species, namely from the *sensu stricto* clade to which also *Lm* belongs. These include the pathogenic species *L. ivanovii*, and the non-pathogenic species *L. innocua*, *L. marthii*, *L. seeligeri* and *L. welshimeri*[24]. Like *Lm*, they all formed VBNC subpopulations in mineral water (Fig. 3a–j). *L. ivanovii* exhibited the greatest drop in culturability (3 log) after 7 days (Fig. 3a), which meant that >99% of viable *L. ivanovii* cells present at day 7 were in a VBNC state (Fig. 3f). *L. marthii* showed transition dynamics similar to *Lm*, with a slower decline in culturability after 7 days (Fig. 3c, compare to Fig. 1b and Supplementary Fig. 4a–d). Finally, *L. innocua*, *L. seeligeri* and *L. welshimeri* displayed intermediate profiles of culturability loss (Fig. 3b, d, e) and VBNC cell formation (Fig. 3g, i, j). The anti-*Lm* antibody also reacted with the CW of these species, so we used it to follow their CW status by fluorescence microscopy. As observed with *Lm*, the other *Listeria* species lost their CW while transitioning to a VBNC state (Fig. 3k–o, u). In parallel, the anti-CWD *Lm* antibody was also able to reveal the gradual exposure of the plasma membrane in these species as they shed their CW (Fig. 3p–u).

Collectively, these results show that the emergence of CWD VBNC forms in mineral water is a transversal phenomenon in *Listeria sensu stricto* species.

Lm adapts its membrane properties to a CWD lifestyle in water

The bacterial CW protects shape and counters the intracellular osmotic pressure, protecting the cell from osmotic lysis. We sought to understand how CWD *Lm* cells can survive in a hypotonic medium, like mineral water, without signs of lysis. We hypothesized that *Lm* may change the properties of its plasma membrane to become more resistant to osmotic pressure before shedding its CW. Indeed, bacteria modulate the fluidity of their plasma membrane, in response to changing environmental factors, to preserve the physical and functional integrity of their interface with the external environment. This is mainly accomplished by changing the fatty acid (FA) composition of membrane phospholipids, which adjusts their degree of packing and, consequently, the fluidity of the membrane[25].

We thus analyzed the FA composition of the *Lm* EGDe membrane by gas chromatography coupled to mass spectrometry. Between day 0 and day 28, we observed a decrease in the relative abundance of anteiso branched-chain species (a-BFA) a-C15:0 and a-C17:0 (Supplementary Fig. 5), which comprise the majority of the *Lm* FA population and are key regulators of membrane fluidity in Gram-positive bacteria[25]. In contrast, linear saturated (SFA) and unsaturated (UFA) FAs showed increased relative levels, mainly on account of C16:0 and C16:1 species (Supplementary Fig. 5). Due to their minor representation in the initial FA population, the fold increase in the SFA and UFA levels was substantial, when compared to the fold change of the more abundant a-BFAs (Fig. 4a). We then investigated if these changes in FA composition were associated with an alteration in the *Lm* membrane fluidity by measuring the generalized polarization (GP) of laurdan, a ratiometric probe that shifts its fluorescence emission peak in response to local membrane phase transitions caused by fluidity changes[26]. An increase of the laurdan GP in labeled *Lm* cells during the first 14 days was suggestive of decreased membrane fluidity (Fig. 4b). To confirm this observation, we directly measured the fluidity-dependent diffusion of the fluorogenic dye Nile red in the *Lm* membrane using total internal reflection fluorescence correlation spectroscopy (TIR-FCS). This technique has been recently implemented to quantify bacterial membrane fluidity in Gram-positive bacteria[27]. TIR-FCS showed a significant reduction of the diffusion coefficient of Nile red in rod-shaped cells between 7 and 14 days (Fig. 4c), suggestive of membrane rigidification. This corresponds to the period when *Lm* is most severely impacted by CW damage and loss (Fig. 1k). Notably, the diffusion coefficient in CWD coccoid cells was similar after 7 or 14 days of incubation in water (Fig. 4c), consistent with increased membrane packing to adapt to a wall-less lifestyle. Furthermore, after 14 days in water, the diffusion coefficient was similar in rod-shaped and coccoid cells, suggesting that the reduction in membrane fluidity occurs prior to CW loss.

Altogether, these findings indicate that *Lm* alters the physicochemical properties of its plasma membrane while transiting to a CWD VBNC state in mineral water. As a result of changes in FA composition, although not excluding the contribution of other membrane components, the membrane becomes more rigid, which may protect the wall-less bacterial cell from osmotic lysis. In agreement with this hypothesis, total *Lm* numbers were notably reduced (2 log) when freshly prepared suspensions were immediately treated with mutanolysin, which digests the *Listeria* CW, without allowing the *Lm* cells to adapt to the hypotonic medium (Fig. 4d). In contrast, bacteria from 28-day-old suspensions were insensitive to this treatment (Fig. 4d).

Stress response plays a role in the formation of CWD VBNC *Lm*

Despite several studies reporting the induction of a VBNC state in *Lm* under different stressful conditions[13,28–33], the molecular factors and pathways involved in this transition remain elusive.

To identify early effectors required for VBNC state transition in mineral water, we analyzed the transcriptional changes in *Lm* EGDe cells after 7 days, when loss of culturability and CW alterations are first observed (Fig. 1). RNA-seq analysis identified a total of 1229 differentially expressed genes (q-value ≤ 0.05, absolute $\log_2$ fold change ≥ 1), of which 593 were downregulated and 636 were upregulated (Fig. 5a; Supplementary Data 1). Gene set enrichment analysis revealed the most prevalent upregulated and downregulated biological processes and pathways. Downregulated genes were found associated with biosynthesis of

https://doi.org/10.1038/s41467-024-52633-7

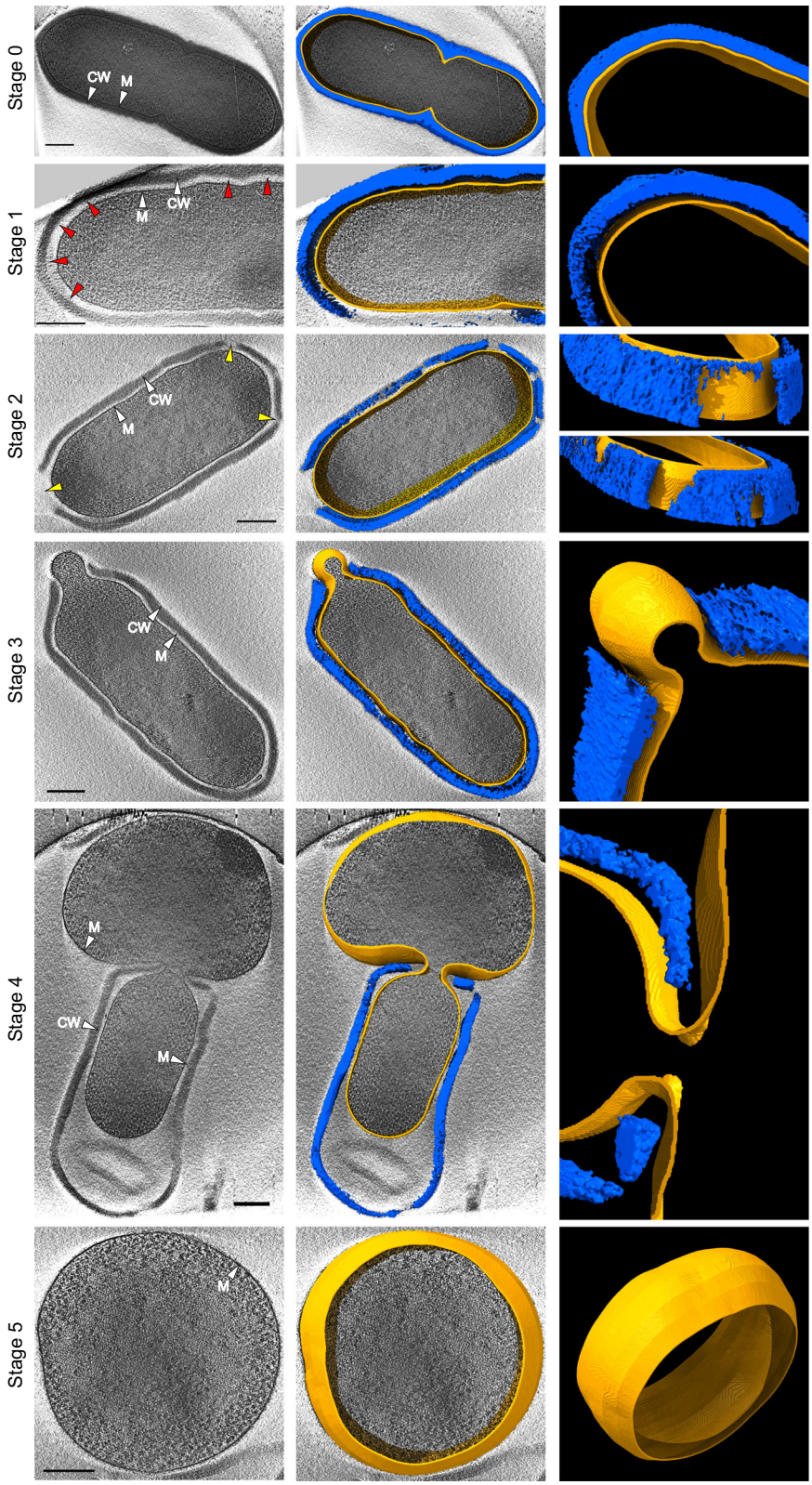

Fig. 2 | Cryo-electron tomography of the *Lm* CW shedding during VBNC state transition. Ultrastructure of the stages of *Lm* CW shedding obtained by cryo-electron tomography of *Lm* EGDe sampled from mineral water at day 0 (stage 0) and day 14 (stages 1–5). Stage 0: a rod-shaped bacterium with tightly connected plasma membrane (M) and CW layers (white arrowheads). In this example, a septum is forming at the midcell region. Stage 1: detachment of the M and CW layers results in the formation of a periplasm-like space (red arrowheads). Stage 2: appearance of CW breaches of variable size (yellow arrowheads) exposes the enclosed protoplast to the extracellular environment. Stage 3: the protoplast begins bulging through a CW breach at one of the poles. Stage 4: the protoplast squeezes out, leaving behind an empty cell wall sacculus. Stage 5: the protoplast has fully egressed from its rod-shaped CW encasing, assuming a coccoid morphology as a CWD form. Left panels: tomogram slice; right panels: 3D rendering of the CW (blue) and M (orange) layers, obtained by manual segmentation of tomogram slices; middle panels: superposition of the tomogram slice and the 3D models. Scale bars: 200 nm. Movies showing all the tomogram slices used for 3D reconstruction of the CW and M layers for stages 0 and 2–5 are available as Supplementary Movies S1–S5.

https://doi.org/10.1038/s41467-024-52633-7

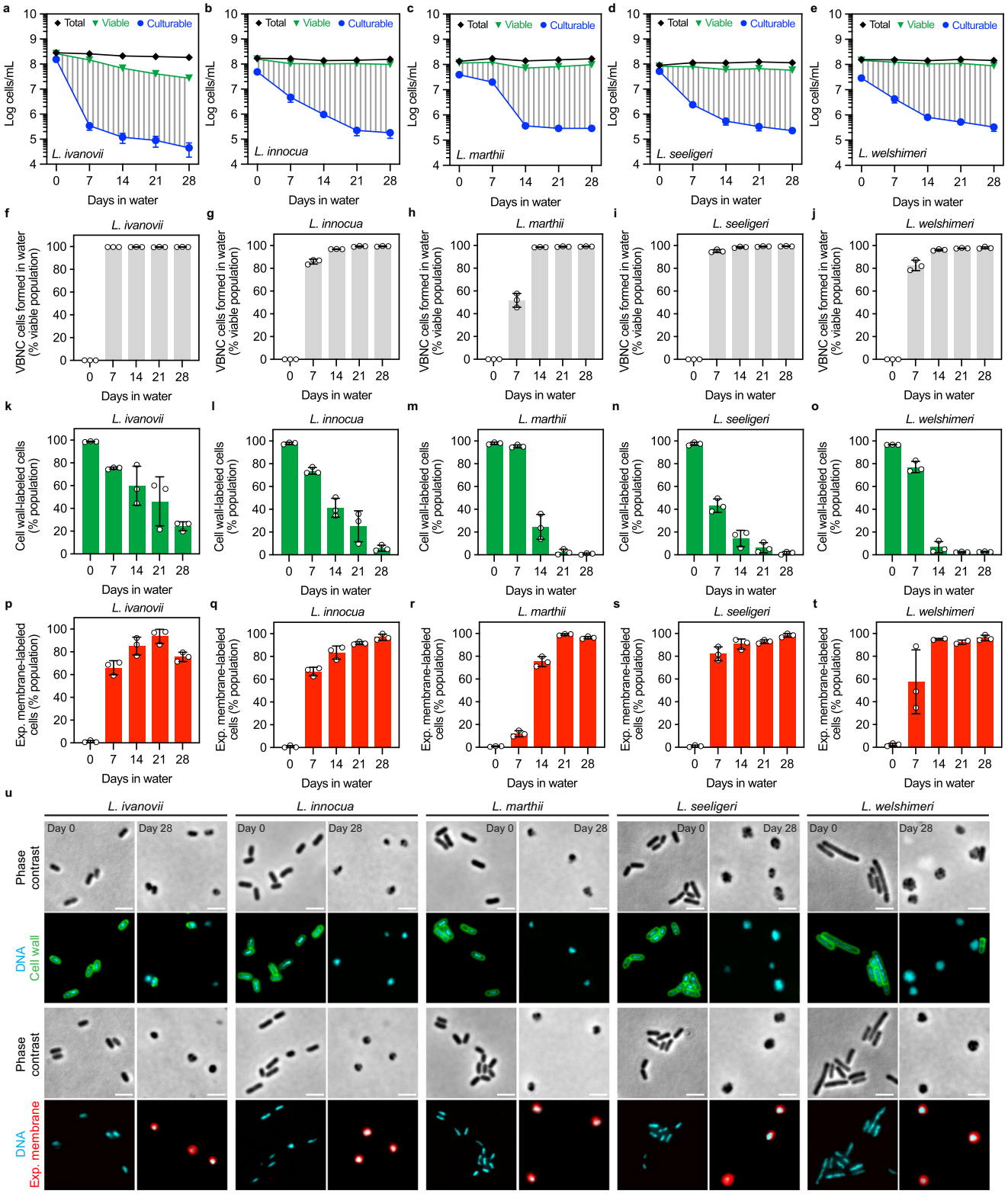

Fig. 3 | A CWD VBNC state occurs in other *Listeria* species. a–e Total, viable and culturable cell numbers of *Listeria sensu stricto* species *L. ivanovii*, *L. innocua*, *L. marthii*, *L. seeligeri*, and *L. welshimeri* in mineral water. Culturable bacteria (blue circles) were quantified by CFU enumeration; total (black diamonds) and viable (green triangles) bacteria were quantified by flow cytometry using CFDA. Dashed area indicates VBNC population. **f–j** Fraction of the viable cell populations shown in **a–e** consisting of VBNC cells formed in mineral water. **k–t** Fraction of the cell populations shown in **a–e** displaying cell wall (**k–o**) or exposed plasma membrane (**p–t**) labeling by fluorescence microscopy. **u** Phase-contrast and fluorescence micrographs of the cell populations quantified in **k–t**. Bacteria were fluorescently labeled for DNA (cyan), cell wall (green), and exposed plasma membrane (red). Data are expressed as mean ± standard deviation of three independently prepared bacterial suspensions (white circles in bar plots). Scale bars: 2 μm. Source data are provided as a Source Data file.

https://doi.org/10.1038/s41467-024-52633-7

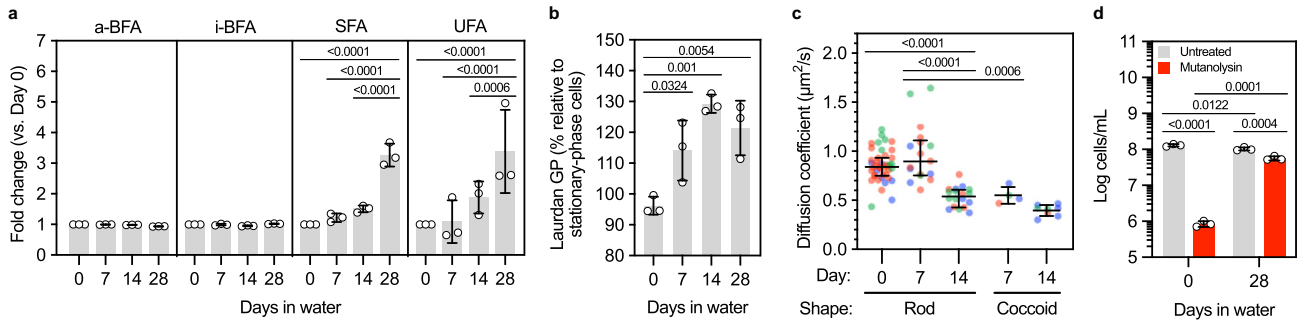

Fig. 4 | *Lm* adapts its membrane properties to a CWD lifestyle. a Fold change of the relative abundance of anteiso-branched (a-BFA), iso-branched (i-BFA), saturated (SFA) and unsaturated (UFA) fatty acids extracted from *Lm* EGDe in mineral water at the indicated timepoints relative to the first timepoint (day 0). Fold change calculated from data in Supplementary Fig. 5. **b** Laurdan generalized polarization (GP) of *Lm* EGDe in mineral water. Increasing relative GP values suggest reduction of the bacterial membrane fluidity. **c** Membrane fluidity of *Lm* EGDe in mineral water. Nile red-stained rod-shaped or coccoid cells were analyzed by total internal reflection fluorescence correlation spectroscopy (TIR-FCS) to determine the membrane-associated dye diffusion coefficient. Each dot represents one measured bacterium, and dots with same color represent bacteria measured from the same suspension. **d** Total cell numbers of *Lm* EGDe in mineral water were quantified by flow cytometry in samples treated (red) or not (gray) with mutanolysin. Data are expressed as mean ± standard deviation (**a**, **b**, **d**) or median + interquartile range (**c**) of three independently prepared bacterial suspensions (white circles in bar plots, differentially colored dots in scatter plot). Statistical significance was determined with two-way ANOVA with Tukey's (**a**) or Šidák's test (**d**), and one-way ANOVA with Dunnett's (**b**) or Tukey's (**c**) tests. Source data are provided as a Source Data file.

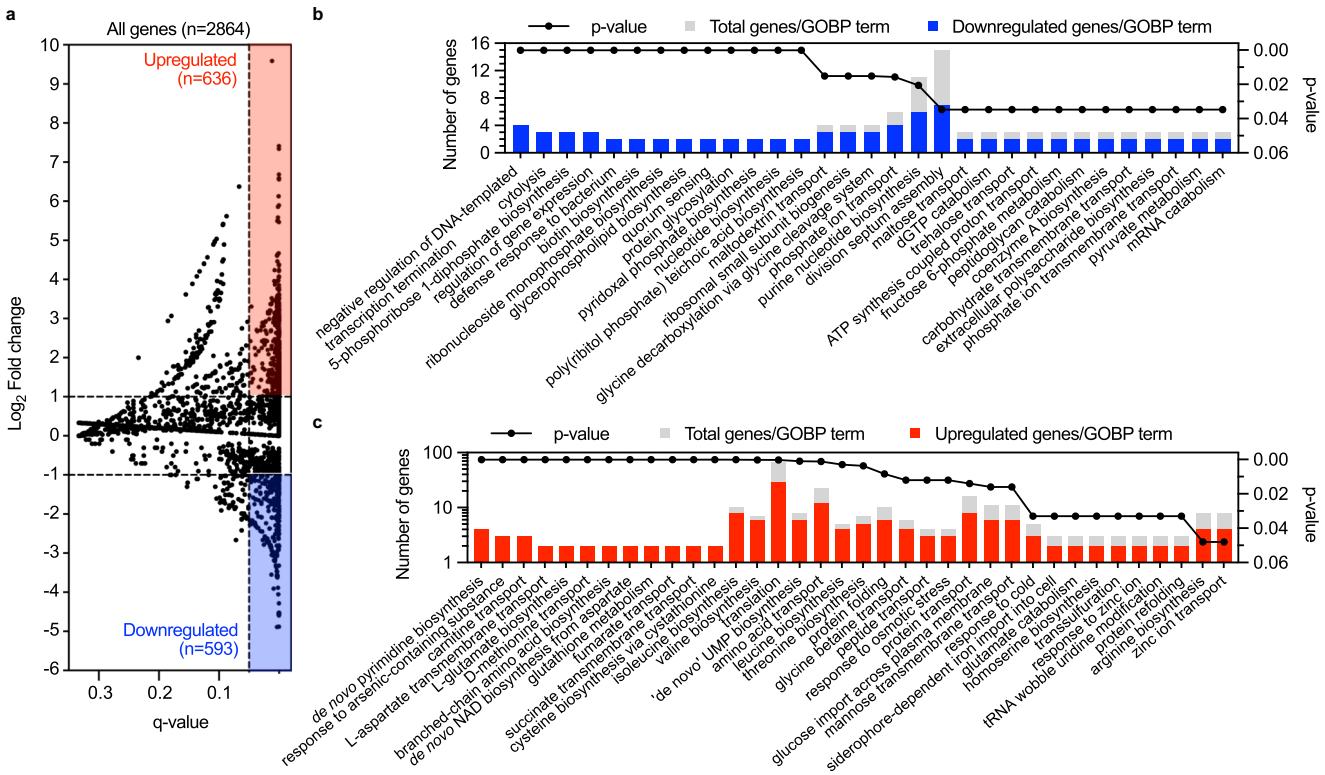

Fig. 5 | Transcriptional reprogramming in the early phase of VBNC *Lm* formation. a Gene expression changes in *Lm* EGDe between 0 and 7 days post-incubation in mineral water. The volcano plot depicts the magnitude ($\log_2$ fold change) and statistical significance (q-value) of the change in transcriptional levels of the *Lm* EGDe genome ($n = 2864$ genes, black dots). Horizontal dashed lines indicate fold change threshold ($|\log_2$ fold change$| = 1$), vertical dashed line indicates statistical significance threshold (q-value = 0.05). Red-shaded area indicates significantly upregulated genes ($n = 636$), blue-shaded area indicates significantly downregulated genes ($n = 593$). **b**, **c** Functional analysis of statistically enriched gene ontology biological process (GOBP) terms in genes downregulated (**b**) and upregulated (**c**) at 7 days. GOBP terms ranked (left to right) by increasing p-value and decreasing fraction of downregulated/upregulated genes per term. Statistical significance was determined with a Benjamini-Hochberg-corrected hypergeometric cumulative probability test[81] (**b**, **c**). Source data are provided as a Source Data file.

nucleotides and coenzymes (biotin, pyridoxal phosphate, coenzyme A), transcription regulation, uptake of phosphate and carbohydrates (maltose/maltodextrin and trehalose phosphotransferase systems), cell envelope assembly (biosynthesis of glycerophospholipids and teichoic acids) and maintenance (peptidoglycan catabolism), cell division (division septum assembly), energy production (pyruvate metabolism, ATP synthesis-coupled proton transport), and protein secretion (Fig. 5b, Supplementary Fig. 6a–c). Upregulated genes were linked with acquisition and/or metabolism of amino acids (aspartate, glutamate, methionine, cysteine, isoleucine, valine, leucine, threonine, arginine); biosynthesis of pyrimidine nucleotides, uptake of carbohydrates (glucose/mannose phosphotransferase systems) and metal ions

(iron, zinc); protein translation and folding, and response to osmotic (transport of compatible solutes carnitine/glycine betaine) and oxidative stress (glutathione metabolism) (Fig. 5c; Supplementary Fig. 6d–f). These results are consistent with a physiological transition taking place in a population of mixed culturable states. Most downregulated genes likely reflect the transition from a vegetative growth state to a VBNC state, whereas most upregulated genes possibly mirror bacterial responses to nutritional and hypoosmotic stresses.

Interestingly, prophage loci were almost completely activated and among the most strongly upregulated genes (Supplementary Data 2), in line with previous reports linking prophage activation with environmental stress[34–37]. In agreement with a stress response activation, nearly half of the regulon controlled by the stress-responsive sigma factor SigB (181 out of 455 genes) was induced (Supplementary Data 3). This elevated number of upregulated SigB-controlled genes prompted us to investigate its involvement in the transition of *Lm* to a VBNC state. We found that SigB-deficient *Lm* EGDe cells transitioned considerably faster than wild-type cells, with a 2-log decline in CFU counts resulting in >90% of viable cells in a non-culturable state after 7 days (Fig. 6a, b). Importantly, >90% of the *Lm* population had already converted to CWD coccoid forms (Fig. 6c, d). These results reveal a major modulating role for SigB in *Lm* adaptation to nutritional deprivation and generation of CWD VBNC forms in mineral water. The unaffected viability of Δ*sigB* cells indicates, however, that SigB is not essential for *Lm* survival in this situation (Fig. 6a).

The stringent response is an important stress signaling mechanism that regulates adaptation to starvation via the alarmone (p)ppGpp[38]. The production of (p)ppGpp was shown to be promoted during transition to a VBNC state, and (p)ppGpp-deficient bacteria were found to lose culturability at a higher rate than their wild-type counterparts[39,40]. Although our transcriptomic data showed no upregulation of the alarmone synthase-encoding genes (*relA*, *relP* and *relQ*) at day 7 (Supplementary Data 1), we examined if the enzymatic activity of these proteins could impact the transition to a VBNC state. Compared to wild-type *Lm* 10403S, a Δ*relAPQ* strain transitioned faster after 7 days (Fig. 6e–h), which was correlated with a statistically significant faster decline of the walled population in the same period (Fig. 6i). This phenotype was rescued by complementation of the mutant strain with either *relA*, *relP* or *relQ* genes (Fig. 6e–i), suggesting a functional redundancy of these enzymes as previously reported[41]. These results suggest that the stringent response plays a role in the early phase of VBNC *Lm* formation.

The autolysin NamA promotes *Lm* CW loss upon VBNC state entry

To gain a molecular insight into the *Lm* CW remodeling dynamics involved in VBNC *Lm* formation in water, we then focused on genes involved in CW metabolism. These genes presented a heterogeneous expression profile, showing either down/upregulation or no change (Supplementary Data 4). Peptidoglycan maturation and turnover is carried out by a family of peptidoglycan hydrolases, commonly called autolysins, that cleave different bonds within the peptidoglycan structure[42]. *Lm* encodes around 20 proteins with confirmed or predicted autolytic activity[43,44]. Our transcriptomic data indicated that many known and putative *Lm* autolysin-coding genes were strongly downregulated after 7 days (e.g. *lmo0394, p60, aut, lmo1215, lmo1521, lmo2522, ami, namA*) (Supplementary Data 4), suggesting that degradation of the CW prior to shedding is carried out efficiently by an existing autolytic activity, without need for additional protein synthesis. We thus tested *Lm* mutants of genes encoding autolysins with different classes of bond-cleaving activity: the DL-endopeptidase p60/Iap, the *N*-acetylmuramoyl-L-alanine amidase Ami, the *N*-acetylglucosaminidases Auto and NamA, and the putative *N*-acetylmuramidases/lytic transglycosylases and resuscitation-promoting factor (Rpf)-like proteins Lmo0186 and Lmo2522[43,45,46].

Lm deficient in p60 (Supplementary Fig. 7a–c) or in both Rpf proteins (Supplementary Fig. 7d–f) showed culturability, VBNC cell formation and CW loss profiles largely similar to those of wild-type bacteria. Ami-deficient *Lm* EGDe showed a higher proportion of walled bacteria at day 14, associated with a delay in culturability decline and formation of VBNC cells at day 7 (Supplementary Fig. 7g–i). Interestingly, in the absence of Auto, *Lm* EGDe presented a significant drop in culturable and walled cell numbers – and thus larger VBNC population – at day 7 (Supplementary Fig. 7j–l).

The most striking phenotype was observed with NamA-deficient *Lm* EGDe, which displayed strongly delayed dynamics of transition to a VBNC state (Fig. 7a–c). Indeed, the culturability of Δ*namA* bacteria was barely affected at day 7 and showed 10-fold higher values than wild-type bacteria at day 14 (Fig. 7a). Importantly, more than 90% of the Δ*namA* population still conserved their CW after 14 days, compared to 44% of wild-type *Lm* (Fig. 7c). As the export of NamA to the bacterial surface is specifically mediated by the accessory Sec system ATPase SecA2[47], we investigated whether SecA2-deficient *Lm* EGDe exhibited a phenotype similar to NamA-deficient *Lm*. Indeed, Δ*namA* and Δ*secA2* bacteria demonstrated very similar dynamics with respect to culturability loss, VBNC cell formation and CW loss, despite substantially lower initial culturable Δ*secA2* counts (Fig. 7d–g). This initial difference is likely due to a division/scission defect of the Δ*secA2* strain that results in a chaining phenotype (Fig. 7g), as SecA2 mediates the secretion of both NamA and p60 autolysins[48]. However, the lack of a role for p60 in CW shedding during VBNC *Lm* formation (Supplementary Fig. 7a–c) suggests that the Δ*secA2* phenotype is caused by the absence of exported NamA. Supporting this hypothesis, CW loss by Δ*secA2* cells was similarly delayed as in Δ*namA* cells (Fig. 7c, f, g). Moreover, while we could not produce a complemented Δ*namA* strain, we were able to complement and rescue the phenotype of Δ*secA2* cells (Fig. 7d–f).

Altogether, these results reveal the *Lm* autolysin NamA as a major player in VBNC *Lm* formation, with an important role in the events tied to CW breakdown and shedding.

VBNC *Lm* reverts back to a vegetative, walled and virulent state

Some bacteria, mostly Gram-negative species, have been shown to exit the VBNC state and regain culturability under specific resuscitation conditions[2,3]. Reversion of the VBNC state in *Lm* and other Gram-positive bacteria remains a challenge[2,49]. Revival attempts through nutrient supplementation (e.g. inoculation into fresh or conditioned medium, pure or diluted) were unsuccessful in our hands (our unpublished results). We thus turned to the chicken embryo model, which was previously used to effectively revive VBNC bacteria, including *Lm*[50–53]. We inoculated embryonated chicken eggs with a suspension of GFP-expressing VBNC *Lm* EGDe containing 10^6 viable cells/mL, of which <1 cells/mL were culturable. In parallel, eggs inoculated with mineral water or with vegetative *Lm* from an overnight broth culture served respectively as negative and positive controls. Two days after inoculation, eggs were processed to assess the presence of culturable *Lm*. All embryonated eggs inoculated with VBNC *Lm* scored positive for bacterial growth (24 out of 24 eggs), similarly to embryonated eggs inoculated with vegetative *Lm* (8 out of 8 eggs). As expected, no bacterial growth was observed in eggs inoculated with mineral water (Table 1).

A critical point with resuscitation of VBNC bacteria is whether the recovered culturable cells resulted from a true revival of VBNC forms or from regrowth of a trace number of culturable cells. To rule out the latter possibility, VBNC *Lm* were inoculated in parallel in BHI, a rich medium that does not support VBNC *Lm* resuscitation[13]. This resulted in bacterial growth in only 9.52% (8 in 84) of inoculated wells, which largely contrasted with growth obtained from 100% of inoculated embryonated eggs. This

https://doi.org/10.1038/s41467-024-52633-7

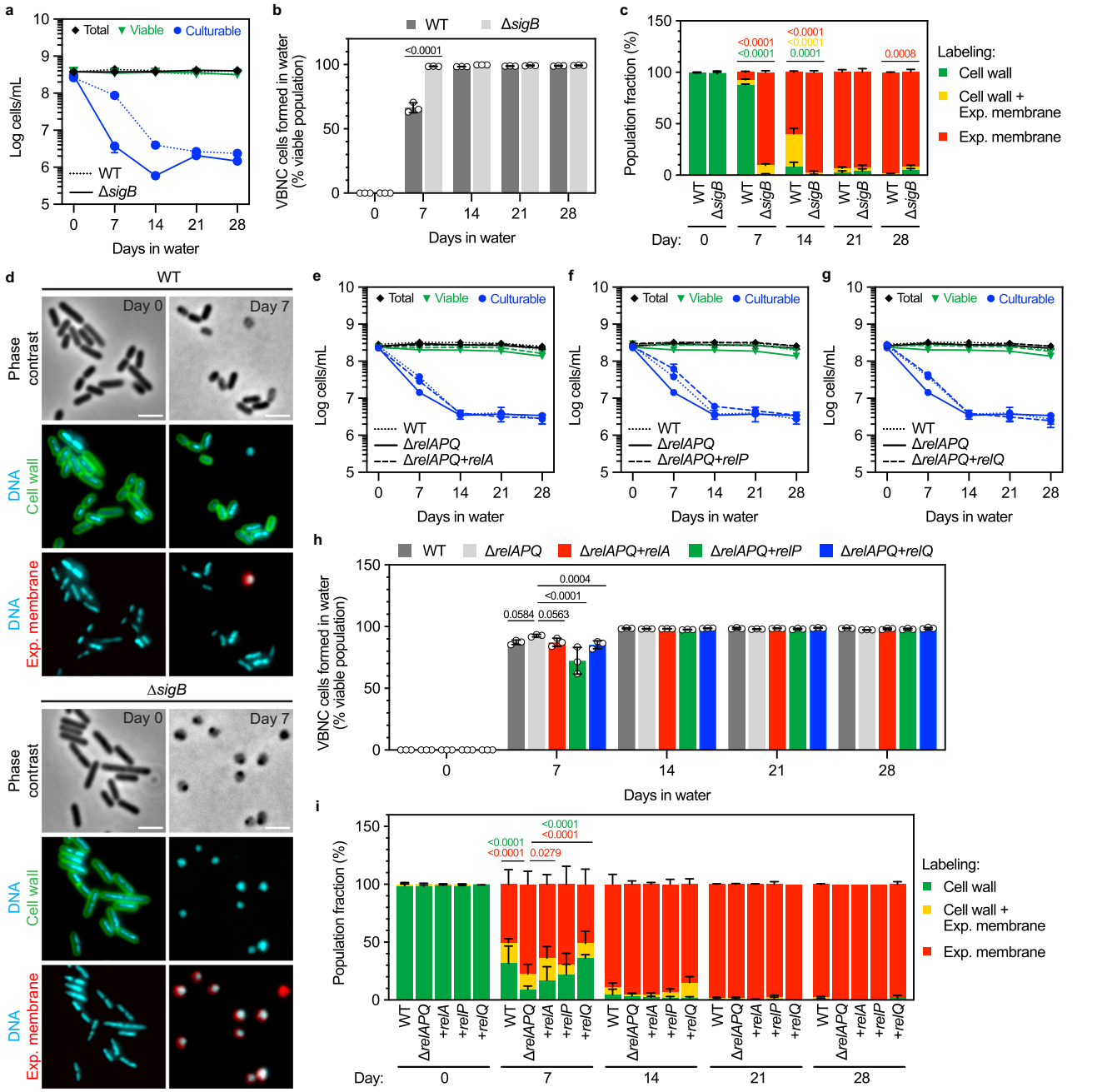

Fig. 6 | SigB and stress response mechanisms modulate the onset of VBNC *Lm* formation. a, **e**–**g** Total, viable and culturable cell numbers of wild-type *Lm* (WT, dotted line), SigB-deficient (Δ*sigB*) and RelAPQ-deficient (Δ*relAPQ*) mutants (solid lines), and complemented Δ*relAPQ* strains expressing *relA* (Δ*relAPQ*+*relA*), *relP* (Δ*relAPQ*+*relP*) or *relQ* (Δ*relAPQ*+*relQ*) (dashed lines), in mineral water. Culturable bacteria (blue circles) were quantified by CFU enumeration; total (black diamonds) and viable (green triangles) bacteria quantified by flow cytometry using CFDA. **b**, **h** Fraction of the viable cell populations shown in **a**, **e**–**g** consisting of VBNC cells formed in mineral water. **c**, **i** Fraction of the cell populations shown in **a**, **e**–**g** displaying single- or double-labeling of cell wall and exposed plasma membrane by fluorescence microscopy. **d** Phase-contrast and fluorescence micrographs of the cell populations quantified in **c**. Bacteria were fluorescently labeled for DNA (cyan), cell wall (green) and exposed plasma membrane (red). Data are expressed as mean ± standard deviation of three independently prepared bacterial suspensions (white circles in bar plots). Statistical significance was determined with two-way ANOVA with Šidák's (**b**, **f**, **i**) or Tukey's (**h**) tests. Scale bars: 2 μm. Source data are provided as a Source Data file.

significantly different proportion of *Lm* growth before and after passage of VBNC cells in embryonated eggs ($p = 1.63 \times 10^{-17}$) attests the successful resuscitation of *Lm* from the VBNC state (Table 1). As a further control, VBNC cells were also inoculated into non-embryonated eggs, which were shown to fail in promoting VBNC *Lm* revival[50]. Whereas vegetative *Lm* were able to proliferate in non-embryonated eggs, we observed no growth coming from VBNC *Lm*-inoculated eggs (Table 1), underlining the requirement of an embryo for VBNC *Lm* resuscitation and further supporting that the revival of VBNC *Lm* in embryonated eggs was not due to residual culturable bacteria in the inoculum.

To confirm if these awakened *Lm* were phenotypically equivalent to vegetative *Lm*, we investigated their morphology and virulence. Fluorescence microscopy of two revived *Lm* clones revealed populations consisting of GFP-expressing, walled, rod-shaped cells that are indistinguishable from vegetative bacteria grown in broth

https://doi.org/10.1038/s41467-024-52633-7

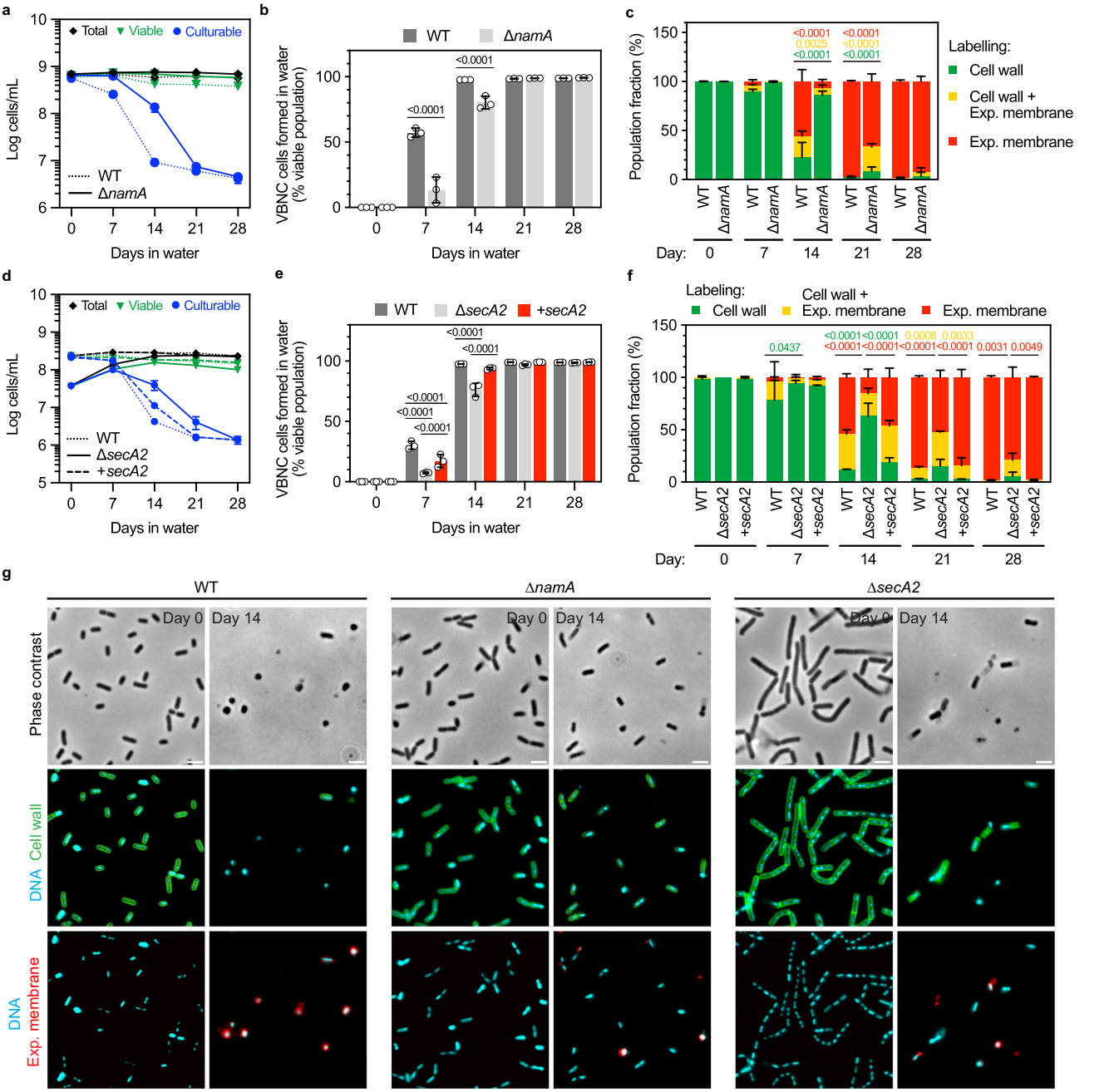

Fig. 7 | The autolysin NamA promotes *Lm* CW shedding and VBNC state entry. a, **d** Total, viable and culturable cell numbers of wild-type *Lm* EGDe (WT, dotted lines), isogenic NamA-deficient (Δ*namA*) and SecA2-deficient (Δ*secA2*) mutants (solid lines), and complemented Δ*secA2* (+*secA2*) strain (dashed line) in mineral water. Culturable bacteria (blue circles) were quantified by CFU enumeration; total (black diamonds) and viable (green triangles) bacteria quantified by flow cytometry using CFDA. **b**, **e** Fraction of the viable cell populations shown in **a**, **d** consisting of VBNC cells formed in mineral water. **c**, **f** Fraction of the cell populations shown in **a**, **d** displaying single- or double-labeling of cell wall and exposed plasma membrane by fluorescence microscopy. **g** Phase-contrast and fluorescence micrographs of the cell populations quantified in **c**, **f**. Bacteria were fluorescently labeled for DNA (cyan), cell wall (green), and exposed plasma membrane (red). Data are expressed as mean ± standard deviation of three independently prepared bacterial suspensions (white circles in bar plots). Statistical significance was determined with two-way ANOVA with Šidák's (**b**, **c**, **f**) or Tukey's (**e**) tests. Scale bars: 2 μm. Source data are provided as a Source Data file.

medium (Fig. 8a). We then assessed the virulence of the revived clones by infecting human trophoblastic (JEG-3) and hepatocytic (HepG2) cell lines. Quantification of the intracellular bacterial load over time revealed no differences between vegetative and revived *Lm* (Fig. 8b). Microscopy analysis of infected cells showed that both revived *Lm* clones produced foci of infected cells after 6 h and spread to the rest of the cell monolayer by 72 h post-infection as efficiently as vegetative *Lm* (Fig. 8c), supported by an equal capacity of polymerizing host actin into propulsive comet-like tails (Fig. 8d).

Altogether, these results provide strong evidence that the CWD VBNC state of *Lm* is fully reversible and bacteria are able to switch back to a walled and cell-infecting state.

Discussion

Lm is a ubiquitous bacterium known to be tolerant to several biotic and abiotic insults. A key factor explaining the presence and survival of this non-sporulating species in a multiplicity of harmful environments is the ability to phase into a dormant VBNC state. This state has been

Table 1 | VBNC *Lm* revert back to a culturable state after passage in embryonated chicken eggs

Inoculum	Culturability before egg passage [a]	Culturability after egg passage [b]			
		Embryonated eggs	*p*-value [c]	Non-embryonated eggs	*p*-value [d]
Mineral water	0/3 (0%)	0/10 (0%)	>0.999	0/10 (0%)	>0.999
VBNC *Lm*	8/84 (9.52%)	24/24 (100%)	1.63×10^{-17}	0/18 (0%)	0.344
Vegetative *Lm*	3/3 (100%)	8/8 (100%)	>0.999	2/2 (100%)	>0.999

[a]Number of BHI wells with bacterial growth/Number of BHI wells inoculated.
[b]Number of eggs with bacterial growth/Number of eggs inoculated.
[c]Comparison of culturability before and after passage in embryonated eggs (two-sided Fisher's exact test).
[d]Comparison of culturability before and after passage in non-embryonated eggs (two-sided Fisher's exact test).

investigated in *Lm* for the past 20 years, namely the abiotic factors driving the formation of VBNC *Lm* in water and other liquid media[12,13,28,54,55], or produce[56]; the virulent and pathogenic status of VBNC *Lm* in cellular and animal models[32,57]; and the conditions for revival of VBNC *Lm*[32,50,56]. The VBNC state in *Lm* remains however a largely uncharacterized phenomenon. In this work, we showed that *Lm* switches from rod-shaped to coccoid cell as it transitions to a VBNC state in mineral water. We further revealed that this coccoid cell form represents a CWD variant that is generated by a molting-like process of CW shedding. Our findings suggest that generation of CWD cells is key for the transition of *Lm* into a non-culturable dormant state in a natural water environment.

The major finding of this work is that CWD VBNC bacteria can naturally emerge and persist in a hypotonic (i.e. osmotically hostile) environment. Following an adaptation period of the initial walled cells to mineral water, the CWD *Lm* forms described in this work are relatively robust in this environment without osmoprotection. This contrasts with other CWD bacterial types, such as L-forms or the recently reported actinomycete S-cells[58], which are formed in an osmoprotective (i.e. hypertonic) environment, or require one during their formation, to avoid explosive cell lysis after CW loss[59]. We also showed that, as *Lm* transitions to a CWD VBNC state, it fine-tunes the physicochemical characteristics of its plasma membrane to become more rigid and potentially more resistant to lysis. It is also possible that physical changes in the cytoplasm could account for the increased mechanical resistance to the extracellular hypoosmotic conditions. To this regard, low metabolic activity has been shown to induce a glassy behavior of the cytoplasm that might help bacteria to preserve their cellular architecture[60].

The CWD *Listeria* described in this study are also distinct from L-forms in their mechanism of formation. Whereas in vitro-generated L-forms are typically induced by artificial weakening/breakdown of the CW (e.g. exposure to antibiotics or lytic enzymes), we show that CWD VBNC *Listeria* arise naturally in mineral water. S-cells were also shown to be naturally formed in response to hyperosmotic conditions; however, unlike CWD VBNC *Listeria*, they did not survive in a hypotonic medium[58]. Notably, *Lm* is ubiquitously found in oligotrophic aquatic environments and its occurrence in environmental surface water samples, for example, is estimated at 10–30% after culturing in selective rich medium[61–64]. The presence of unculturable CWD *Lm* in these environmental niches may therefore be vastly underestimated. In this regard, the antibodies generated in this study that specifically recognize wall-less VBNC forms of different *Listeria* species, including the two pathogenic *Lm* and *L. ivanovii*, constitute a biomolecular tool with potential use in the detection of dormant pathogens, otherwise untraceable by standard growth-based techniques.

Cryo-ET characterization of the *Lm* CW shedding process showed the extrusion of the bacterial protoplast through one of many breaches in the CW sacculus. A similar process was notably first observed in *Bacillus subtilis* cells transitioning to an L-form state[16], which suggests common mechanisms underlying the CW loss event in both species. Indeed, perturbations in CW loss affected the production of *B. subtilis* L-forms[16] as well as of VBNC *Lm* in water. Mutations in *B. subtilis* genes resulting in sustained autolysin activity and/or septum malformation were found to promote CW extrusion and L-form emergence[16]. Interestingly, we identified the *Lm* autolysin NamA as an important player in this process, since NamA-deficient cells were strongly delayed in CW shedding and VBNC state entry. Highlighting this importance, NamA is widespread in *L. monocytogenes* and other *Listeria* species, with a high protein conservation degree (>90% similarity in >68 strains)[65]. Among the other tested autolysins, only Ami promoted the *Lm* CW shedding process, although at a less significant level compared to NamA. An in-depth screening of the *Lm* autolysin collection should reveal the full list of peptidoglycan-degrading enzymes involved in the formation of CWD VBNC *Lm*.

Inactivation of the *Lm* general stress response or the stringent response, via genetic deletion of the transcription factor SigB or the (p)ppGpp synthetases (RelAPQ), resulted in unexpectedly faster dynamics of VBNC cell formation. This phenotype was particularly strong in SigB-deficient cells, almost completely wall-less after just 7 days. Intriguingly, the absence/misregulation of these important stress response systems did not affect *Lm* cell viability, indicating that they are not required for bacterial survival in a rather stressful context. These results suggest that stress response regulators may secure a balance between vegetative and dormant states; in mineral water, the absence of these regulators might break the balance in favor of transition to the VBNC state. It will be interesting to understand whether the lack of SigB or a functional stringent response in these mutant bacteria has deleterious consequences, for example in their capacity to successfully exit the VBNC state.

We then showed that CW shedding during transition to a VBNC state is not limited to *Lm* and can occur in other pathogenic and non-pathogenic *Listeria* species. This may thus represent an evolutionary strategy within the *Listeria* genus to withstand prolonged nutritional deficiency. It has been hypothesized that the bacterial CW primarily evolved as a structure for storage of sugar- and amino acid-rich components[59]. Breakdown and salvage of CW components could constitute a bacterial mechanism to secure nutrients to sustain a minimal metabolic flux through the unknown duration of a VBNC state. Whether this ability to form wall-less dormant forms in similar conditions also extends to other species from phylogenetically related genera, including sporulating species, remains to be investigated.

Many pathogenic bacteria have been reported to transition to a VBNC state and, for some, this is associated with a loss of virulence[66]. We showed that CWD VBNC *Lm* reverted to a culturable state and recovered its CW and virulence, after passing through the chicken embryo. This indicates that one or more yet-unidentified signals present in this host environment can wake up these dormant *Lm* forms. Similar resurrection signals might be present in other eukaryotic hosts and in nature, and their identification constitutes a challenging but exciting research avenue.

It is becoming clear that a CWD state is an alternative lifestyle that enables bacteria to survive under stress and even proliferate without the mechanical protection of a rigid CW[58,59]. The emergence

https://doi.org/10.1038/s41467-024-52633-7

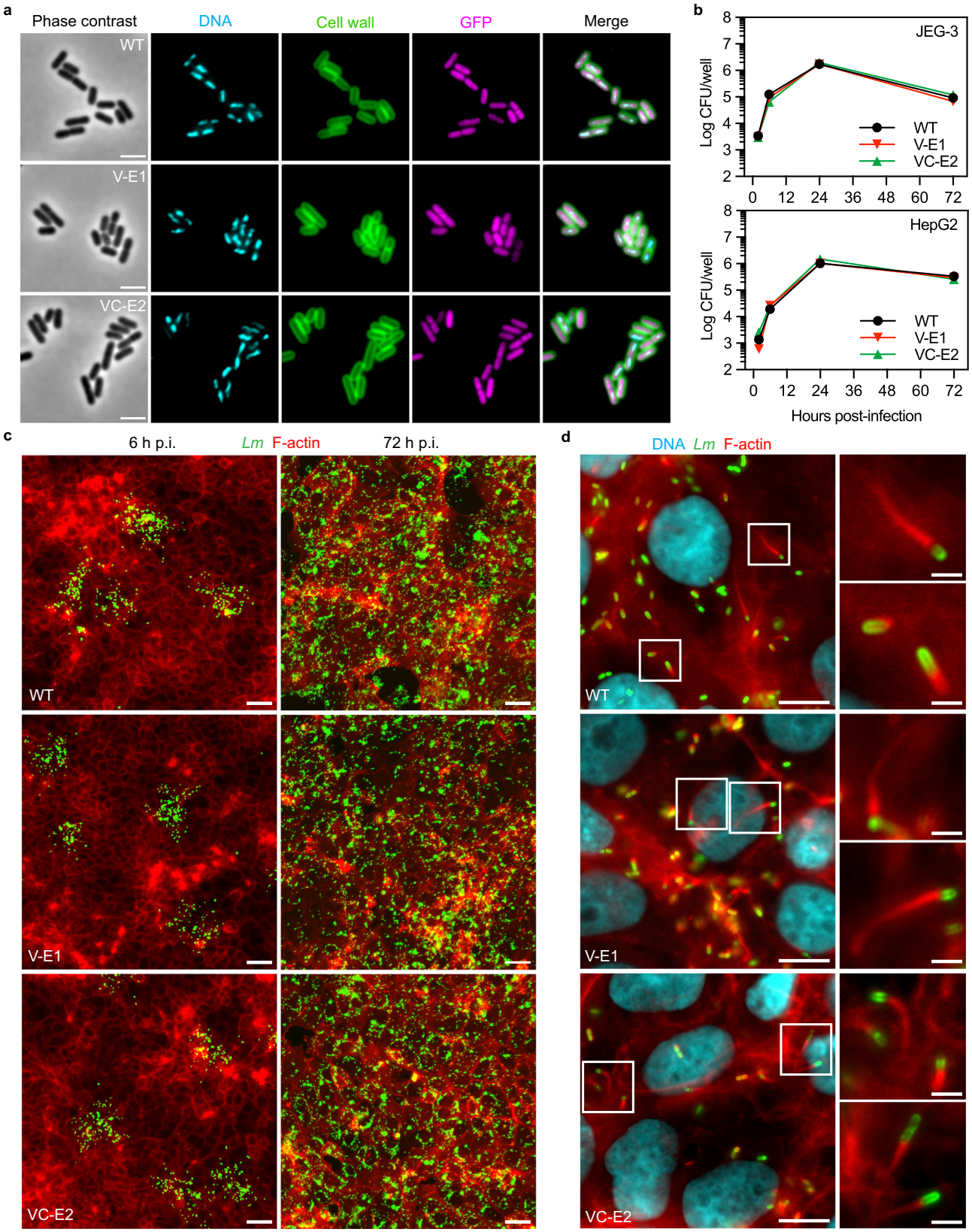

of CWD forms in phylogenetically distant bacterial species[58,67,68] raises the possibility that transient CW loss may be a more common phenomenon among bacteria than expected. In a world dominated by walled microbes, a temporary wall-less state of dormancy might represent a strategy to promote bacterial persistence under harsh environmental contexts.

Methods

Ethics statement

Experimentation with chicken embryos followed all applicable institutional, French (Decree no. 2013-118) and European (Directive 2010/63/EU) guidelines. Since embryos were manipulated and euthanized before the last third of the chicken embryonic development period

Fig. 8 | Chicken embryo passage restores culturability and virulence to VBNC *Lm*. **a** Phase-contrast and fluorescence micrographs of GFP-expressing *Lm* EGDe before (WT) and after VBNC state entry in mineral water and passage through embryonated chicken eggs (clones V-E1 and VC-E2). Bacteria were fluorescently labeled for DNA (cyan) and cell wall (green). **b** Intracellular replication of WT (black circles and line), V-E1 (red down-pointed triangles and line) and VC-E2 (green up-pointed triangles and line) in human epithelial JEG-3 and HepG2 cell lines. Intracellular viable bacteria were quantified by CFU enumeration from agar medium-plated cell lysates. **c** Low-magnification fluorescence micrographs of JEG-3 cell monolayers infected with WT, VE-1 or VC-E2, showing cell-to-cell spread of intracellular bacteria between 6 h (isolated clusters of infected cells) and 72 h post-infection (generalized infection of the cell monolayer). Cells were fluorescently labeled for *Lm* (green) and F-actin (red). Bacteria-associated fluorescence signal was digitally enhanced for clarity. **d** Fluorescence micrographs showing WT, VE-1 and VC-E2 in the cytoplasm of infected JEG-3 cells at 6 h post-infection. Cytosolic *Lm* polymerize host actin into comet-like tail structures that promote intracellular motility and subsequent intercellular spread. Cells were fluorescently labeled for DNA (cyan), *Lm* (green) and F-actin (red). Bacteria highlighted in white squares are shown enlarged in right-side panels (nuclei omitted for better visualization of bacteria and actin tails). Data are representative of one (**a**) or two (**b**–**d**) experiments. Scale bars: 2 μm (**a**;**d**, inset panels), 50 μm (**c**), and 10 μm (**d**, left panels). Source data are provided as a Source Data file.

(i.e. 14 days), the experimental protocols were not subject to acceptance by an ethics committee, according to French legislation (Decree no. 2020-271).

Bacterial strains, cell lines, and growth conditions

Bacterial strains used in this work are listed in Supplementary Table 2. Complementation of the Δ*secA2* mutant strain was achieved by transformation of electrocompetent bacteria[69] with the chromosome-integrative pPL2 plasmid[70] containing a DNA insert with the native *secA2* promoter and protein-coding sequences. This insert was amplified by PCR from *Lm* EGDe genomic DNA (forward primer: 5'-CGC GGATCCGTAAACCTTTATAGTG-3'; reverse primer: 5'-CGCGTCGACT TAGCCTTGGATTAAG-3') and cloned into the *Bam*HI and *Sal*I sites of pPL2. Bacteria were grown under agitation at 37 °C in brain and heart infusion (BHI) broth (BD Bacto, #237500) and agar (BD Difco, #241830) media.

Cell lines of human origin used in this work included JEG-3 trophoblasts (ATCC HTB-36), cultivated in MEM (Thermo Fisher Scientific, Gibco, #41090) supplemented with 10% (v/v) fetal calf serum (Eurobio Scientific, #CVFSVF00-01), and HepG2 hepatocytes (ATCC HB-8065), cultivated in DMEM (Thermo Fisher Scientific, Gibco, #61965) supplemented with 10% (v/v) fetal calf serum. Cells were incubated at 37 °C in a humidified (90–95%) atmosphere with CO_2 at 5% (for cell propagation) or 10% (for infected cells).

Preparation of bacterial suspensions in mineral water

Bacterial suspensions in mineral water were prepared with bacteria from overnight-grown stationary-phase cultures. For each tested species, the bacterial concentration of stationary-phase cultures was determined beforehand by enumeration of colony-forming units (CFU) after plating in agar media. Bacteria were pelleted by centrifugation (3000 × *g*, 5 min) and washed with 1 volume of sterile-filtered (0.22 μm) mineral water (henceforth referred simply as mineral water) for three times before resuspension in 1 volume of mineral water. Washed bacteria were then set to the desired concentration in a final volume of 30 mL of mineral water, and incubated statically at room temperature in an upright-standing, sterile tissue-culture flask (25 cm^2, vented cap). Samples were collected for downstream analyzes immediately after preparation (day 0) and after 7, 14, 21 and 28 days.

Bacterial culturability and viability assays

Bacterial suspensions were regularly sampled for monitorization of the total, viable and culturable cell populations. The culturable population was quantified through enumeration of CFU following the plating of serial dilutions of the suspension on agar media. The total and viable populations were quantified by flow cytometry using a CytoFLEX S analyzer (Beckman Coulter, model V0-B2-Y4-R0) equipped with three excitation lasers (405, 488 and 561 nm) and operated by the CytExpert software (Beckman Coulter, v2.4).

Suspensions prepared at 10^8 cells/mL were ten-fold diluted in mineral water before acquisition at a flow rate of 10 μL/min. Bacteria-associated events were detected in a forward scatter (FSC) versus side scatter (SSC) plot (Supplementary Fig. 1a) and the total population was quantified by enumeration of FSC/SSC-gated events in a defined sample volume (10 μL). For determination of viable population using viability dyes, diluted suspensions were incubated in the dark either with 30 μM 5(6)-carboxyfluorescein diacetate (CFDA, Sigma-Aldrich, #21879) for 30 min or with a mix of 3.34 μM SYTO 9 and 20 μM propidium iodide (PI) from the LIVE/DEAD BacLight Bacterial Viability kit (Thermo Fisher Scientific, Molecular Probes, #L7012) for 15 min. Fluorescence emission by CFDA, SYTO 9 (525/40 nm bandpass) and PI (690/50 nm bandpass) was detected from FSC/SSC-gated bacteria, and populations containing viable (i.e. $CFDA^+$ or SYTO $9^+/PI^-$) or injured/dead bacteria (i.e. $CFDA^-$ or PI^+) were gated with the help of a dead bacteria control sample consisting of heat-treated (95 °C, 30 min) bacterial suspension (Supplementary Fig. 1a). The viable population was quantified by enumeration of $CFDA^+$ or SYTO $9^+/PI^-$-gated events in a defined sample volume (10 μL).

Intracellular ATP quantification

The intracellular ATP content of bacteria suspended in mineral water was determined using the luciferase-based BacTiter-Glo Microbial Cell Viability Assay kit (Promega, #G8230). As per the manufacturer instructions, 100 μL of bacterial suspension were mixed in an opaque white 96-well plate with 100 μL of room temperature-equilibrated BacTiter-Glo Reagent, and incubated in the dark for at least 5 min. Relative luminescence units (RLU) were then recorded in an Infinite M200 microplate reader (Tecan) controlled by i-control software (Tecan, v3.9.1.0) with a 1-second integration time per well. Wells containing mineral water were used to record background luminescence.

Peptidoglycan extraction and UHPLC analysis

Peptidoglycan was extracted from *Lm* EGDe as described[71]. Bacteria (10^{11} cells) were harvested from mineral water suspensions (10^8 cells/mL) on the day of preparation (day 0) and after 7 and 28 days by centrifugation (4000 × *g*, 5 min), flash-frozen in liquid nitrogen and stored at −80 °C until further processing. Each bacterial cell pellet was then resuspended in 40 mL of cold distilled water, boiled for 10 min, cooled, and centrifuged. After suspending the cell pellet in 1 mL of distilled water, 1 mL of SDS solution (10% SDS in 100 mM Tris-HCl pH 7.0) at 60 °C was added and the suspension was boiled for 30 min and centrifuged (20 min, 25,000 × *g*). The pellet was resuspended in 2 mL of lysis solution (4% SDS in 50 mM Tris-HCl pH 7.0), boiled for 15 min, and washed six times with 60 °C-heated distilled water. Next, the pellet was treated with 2 mg/mL of pronase from *Streptomyces griseus* (Roche, #10165921001) in 50 mM Tris-HCl pH 7.0 for 1.5 h at 60 °C, and afterwards with 10 μg/mL of DNase I (Thermo Fisher Scientific), 50 μg/ml of RNase (Thermo Fisher Scientific) and 50 μg/mL lipase from *Aspergillus niger* (Sigma-Aldrich, #62301) in a buffer solution (20 mM Tris-HCl pH 7.0, 1 mM $MgCl_2$, 0.05% sodium azide) for 4 h at 37 °C. The suspensions were washed with distilled water and treated with 200 μg/mL of trypsin (Sigma-Aldrich) in 20 mM Tris-HCl pH 8.0 overnight at 37 °C with agitation. Finally, after inactivating trypsin (3-min boil), the suspensions were incubated with 48% hydrofluoric acid (Merck) overnight at 4 °C. After centrifugation (20 min, 25,000 × *g*), the pellet was washed twice with 250 mM Tris-HCl pH 7.0

and four times with distilled water to raise the pH to 5. The extracted peptidoglycan was lyophilized and resuspended in distilled water.

Muropeptides were prepared from purified peptidoglycan by overnight digestion with 2500 U/mL mutanolysin (Sigma-Aldrich, #M9901) in 25 mM $NaHPO_4$ pH 5.5, at 37 °C with shaking. After reduction with sodium borohydride, muropeptide originating from peptidoglycan extracted from the same number of cells (1.5×10^9) were analyzed by reverse phase-ultra high-pressure liquid chromatography (RP-UHPLC) using a 1290 chromatography system (Agilent Technologies) equipped with a Zorbax Eclipse Plus C18 RRHD column (100 × 2.1 mm, 1.8-µm particle size; Agilent Technologies) and operated by Open Lab CDS ChemStation Edition software (Agilent, rev.C01.03). Elution was performed at 50 °C with 10 mM ammonium phosphate pH 5.6 and a linear gradient (0–20%, 270 min) of methanol, at a flow rate of 0.5 mL/min. Eluted muropeptides were detected by absorbance (202 nm).

Gentamicin protection assay

JEG-3 and HepG2 cell lines were seeded in 24-well plates, with or without coverslips, to reach 90–100% confluency on the day of infection. Prior to seeding HepG2 cells, wells and coverslips were surface-coated with type-I collagen (Sigma-Aldrich, #C3867) in a 50 µg/mL solution in Dulbecco's phosphate-buffered saline (DPBS; Thermo Fisher Scientific, Gibco, #14190) for 30 min and washed once with DPBS. On infection day, bacterial inocula were prepared by washing bacteria from overnight-grown, stationary-phase BHI cultures with DPBS and diluting them in serum-free medium. Cell monolayers were washed once with serum-free medium and infected for 1 h with the inocula at a multiplicity of infection (MOI) of 0.01 bacteria/JEG-3 cell or 5 bacteria/HepG2 cell. The inocula were removed from the wells and replaced with serum-supplemented medium containing 25 µg/mL of gentamicin (Sigma-Aldrich, #G1397), to kill non-internalized bacteria. At 2 h, 6 h, 24 h and 72 h post-infection, cells were processed for immunofluorescence (see below) or for quantification of intracellular viable bacteria. In the latter case, cells were lysed in cold distilled water and serial dilutions of the lysates in DPBS were plated on BHI agar and incubated at 37 °C for at least 24 h for CFU enumeration.

Generation of a polyclonal antiserum against CWD *Lm*

A rabbit polyclonal antiserum was raised against CWD *Lm* as follows. *Lm* 10403S were suspended in mineral water (10^8 bacteria/mL), as described above, and incubated for 42 days. Bacteria were harvested by centrifugation (8000 × *g*, 5 min), resuspended and incubated in fixative solution (1% (v/v) paraformaldehyde (PFA) in DPBS) at 32 °C for 2 h, washed three times and resuspended in DPBS. Bacterial neutralization was confirmed after plating on BHI agar and incubation at 37 °C for several days.

Animal immunizations and serum recovery were outsourced (Covalab, Bron, France). White New Zealand female rabbits were inoculated with 1 mL of a 1:1 mixture of 10^8 PFA-fixed CWD *Lm* and incomplete Freund's adjuvant, and received boosts every three weeks for a total of three boosts. Immune serum was harvested at 53 and 74 days post-immunization and its reactivity and specificity towards CWD *Lm* was assessed by immunofluorescence microscopy.

Immunofluorescence microscopy

Bacterial cells spotted onto poly-L-lysine-treated coverslips or coverslip-attached eukaryotic cells were fixed in a 4% (v/v) PFA solution in DPBS for 20 or 30 min, respectively. Cells were washed in DPBS, incubated in a blocking solution (2% bovine serum albumin in DPBS) for 20 min and, in the case of eukaryotic cells, permeabilized (in a 0.4% (v/v) Triton X-100 solution in DPBS for 4 min, followed by three washes in DPBS) before proceeding with fluorescent labeling.

Rabbit *Listeria* O Antiserum Poly (anti-*Lm*; BD Difco, #223021) was used (1:1000 dilution) to label the CW of *Listeria*. Oregon Green 488- or TRITC-conjugated WGA (Thermo Fisher Scientific, Molecular Probes, #W7024) was used (25 µg/mL) to label the CW of serogroup 1/2 *Lm* strains (EGDe, 10403S). The generated rabbit anti-CWD *Lm* antiserum was used (1:1000 dilution) to label the exposed protoplast membrane of CW-shedding or CWD *Listeria*. Secondary antibodies (1:400 dilution) consisted of goat and alpaca anti-rabbit antibodies conjugated with Alexa Fluor 488 (Jackson ImmunoResearch, #111-545-003), Cy3 (Jackson ImmunoResearch, #611-165-215) or Cy5 (Jackson ImmunoResearch, #111-175-3144). Alexa Fluor 647-conjugated phalloidin (Thermo Fisher Scientific, Molecular Probes, #A22287) and Hoechst 33342 (Sigma-Aldrich, #B2261) were respectively used to label F-actin and DNA, and, as with WGA, were added together with secondary antibodies. All incubations were made in blocking solution for 1 h in the dark.

Samples were mounted onto microscope glass slides with Fluoromount-G medium (Thermo Fisher Scientific, Invitrogen, #00-4958-02) and examined on a ZEISS Axio Observer.Z1 epifluorescence microscope equipped with Plan-Apochromat 20×/0.8 NA (non-immersion), 40×/1.3 NA Oil and 100×/1.4 NA Oil (immersion) objectives, an Axiocam 506 Mono camera and operated with ZEN 2012 Blue software (Carl Zeiss Microscopy, v2.0.0.18). Three to seven fields were acquired per coverslip and images were processed for quantification (see below) and/or figure montage with Fiji software.

Image quantifications

Bacterial cell morphology was analyzed using Fiji software (http://imagej.net/software/fiji, v1.54)[72] as follows: automatic thresholding was applied to phase-contrast images to select objects, and particle length and roundness parameters were selected ("Fit ellipse" and "Shape descriptors" options in "Set Measurements" menu) to be measured on thresholded objects ("Limit to threshold" option in "Set Measurements" menu). Outlier objects (i.e. too small/big, irregularly shaped) were excluded from the particle analysis (size: 0.5–1.5 µm^2, circularity: 0.1–1.0). The length and roundness values per measured object were retrieved from the results table under the "Major" and "Round" columns, respectively.

To quantify the fraction of bacterial populations with CW and/or exposed plasma membrane (i.e. single or double) labeling, phase-contrast channel images were thresholded to select phase-contrast dense objects. Object outlines were then first laid over the DNA fluorescence channel to select bacterial cells, and afterwards over the fluorescence channels associated with CW and/or exposed plasma membrane to enumerate bacteria with single/double labeling. As co-labeling with the anti-*Lm* and anti-CWD *Lm* antibodies was not possible (same host species), only single-labeling quantifications were performed from separately labeled samples of the same bacterial population.

Cryo-electron tomography

A solution of bovine serum albumin-coated gold tracer containing 10-nm colloidal gold fiducial particles (Aurion) was mixed with bacterial suspensions at a 2:1 ratio. This mixture was applied to the front (3.7 µL) and to the back (1.3 µL) of carbon-coated copper grids (R2/2, Cu 200 mesh; Quantifoil) previously glow-discharged (2 mA, 1.8×10^{-1} mbar, 1 min) in an ELMO system (Cordouan Technologies). Excess liquid was removed by blotting the grid backside with filter paper (9 sec, 18 °C, 95% humidity) and the sample was immediately frozen in liquid ethane in an EM GP automatic plunge freezer (Leica Microsystems). Grids were stored in liquid nitrogen until image acquisition.

Tilt series were acquired in a 300 kV Titan Krios G3 transmission electron microscope (Thermo Fisher Scientific), equipped with a Cold FEG tip, a Selectris X energy filter with slit width set to 20 eV, single-tilt axis holder and a Falcon 4i direct electron detector (Thermo Fisher Scientific), and operated with the SerialEM software (U. Colorado Boulder, USA, v4.0.13)[73]. Tilt series acquisition was performed in

batches using a dose-symmetric scheme. One batch was obtained with an angular range of ± 42° (3° increment), a defocus range from −3 to −8 μm, a pixel size of 4.8 Å (26,000× magnification), an exposure time of 8 s, a dose rate of 13.7 e/pixel/s and a total electron dose of about 140 e/Å^2. Another batch was acquired with an angular range of ± 50° (2° increment), a defocus range from −3 to −8 μm, a pixel size of 6.4 Å (19,500× magnification), an exposure time of 10 s, a dose rate of 12 e/pixel/s and a total electron dose of about 150 e/Å^2. Tilt series were saved as separate stacks of frames, motion-corrected and restacked in order using the *alignframes* module in SerialEM.

3D reconstructions of tomograms were calculated in IMOD software (U. Colorado Boulder, USA, v4.9.10)[74] by weighted back projections with dose weighting and a SIRT-like filter. The IMOD drawing tools and interpolator module were used to manually trace and produce a 3D surface of the bacterial plasma membrane. This surface was then imported to ChimeraX software (UC San Francisco, USA, v1.5)[75] and used as a mask to extract slabs of subvolumes corresponding to the bacterial plasma membrane and CW. For the plasma membrane subvolume, the slab was produced using the *volume onesmask* function. For the CW, the *volume mask* function was used instead, cropping a larger slab beyond the CW limits, and the subvolume was visualized using the isosurface representation with an appropriate intensity threshold. Final visualizations and rendering were performed in ChimeraX using homemade scripts for video production.

Fatty acid extraction and GC-MS analysis

Bacteria were harvested by centrifugation (3000 × *g*, 5 min), flash-frozen in liquid nitrogen and stored at −80 °C until further processing. Extraction and methylation of fatty acids (FA) were carried out directly on bacterial pellets as described[76]. Whole-cell FA were first saponified and esterified by methanolic NaOH (1 mL of 3.75 M NaOH in 50% (v/v) methanol for 30 min at 100 °C) followed by methanolic HCl (addition of 2 mL of 3.25 M HCl in 45% (v/v) methanol solution and incubation for 10 min at 80 °C). FA methyl esters (FAME) were then extracted with a 1:1 (v/v) diethyl ether/cyclohexane solution, and the organic phase was washed with dilute base (0.3 M NaOH).

Analytical gas chromatography of FAME was carried out in a GC-MS Trace 1300 / ISQ 7000 system (Thermo Fisher Scientific) equipped with a BPX70 capillary column (25 m, 0.22-mm internal diameter; SGE, Victoria, Australia). Column temperature was set at 100 °C for 1 min and then increased to 170 °C at a rate of 2 °C/min. FA species were identified using MS databases (Replib, Mainlib, FAME2011). The relative abundance of FA species was expressed as the percentage of the total FAME peak area. Identified FA species were grouped in the following classes: iso and anteiso branched-chain FA (i-BFA and a-BFA), saturated FA (SFA), and unsaturated FA (UFA).

Laurdan generalized polarization

The generalized polarization of the lipophilic dye laurdan (6-dodecanoyl-2-dimethylaminonaphthalene), when bound to the *Lm* plasma membrane, was used as a measure of the bacterial membrane fluidity[26]. Bacteria were sampled (1 mL) from mineral water suspensions (10^8 cells/mL) at 0, 7, 14 and 28 days and incubated for 10 min in the dark with 10 μM of laurdan (Sigma-Aldrich, #40227) from a 1 mM stock in dimethylformamide (DMF). Unbound laurdan was washed off of bacterial cells with four cycles of centrifugation (8000 × *g*, 5 min) and resuspension (vortex) in 1% (v/v) DMF in mineral water. After a final resuspension (vortex) in 1 mL of the washing solution, technical replicates (200 μL) were added to a clear-bottom black 96-well plate, which was then equilibrated to 25 °C in a Spark microplate reader operated by SparkControl software (Tecan). After equilibration, laurdan fluorescence emission was induced at 350 nm and recorded at 450 and 500 nm. The generalized polarization (GP) of laurdan was determined by the formula: $GP = (I_{450} - I_{500})/(I_{450} + I_{500})$, where I corresponds to the fluorescence intensity value at the recorded emission wavelength[26]. The GP values obtained for every timepoint were normalized to those obtained from bacterial suspensions prepared on the same day (i.e. day 0). An increase of normalized laurdan GP values can be interpreted as a reduction of plasma membrane fluidity.

TIR-FCS

The diffusion of the lipophilic dye Nile red in the membrane of *Lm* was measured using total internal reflection fluorescence correlation spectroscopy (TIR-FCS)[77]. In short, bacterial cells were labeled for 10 min with 0.1 μg/mL of Nile red (Sigma-Aldrich, #72485) from a 50 μg/mL stock in DMSO. TIR-FCS acquisitions were performed with a ZEISS Elyra PS1 TIRF microscope equipped with a Plan-Apochromat 100×/1.46 NA Oil immersion objective (Carl Zeiss Microscopy) and operated with ZEN 2012 SP2 Black (Carl Zeiss Microscopy, v11.0.0.0). Fluorescence excitation at 561 nm was set to a power of ~70 nW/μm². Each FCS acquisition consisted of a stack of 50,000 frames with a frame acquisition time of 1.26 ms, maximized by the use of only 10 lines of the camera chip. Pixels were binned 2 by 2 to increase signal levels to an effective pixel size of 320 nm. The resulting intensity timetraces were correlated and fitted using the open-source Python package PyimFCS software (http://github.com/aurelien-barbotin/pyimfcs) as described[77].

TIR-FCS estimation of diffusion coefficients in small cells, such as bacteria, is biased by the cell morphology[77]. To correct for this bias, the cell width and length of Nile red-stained bacteria were measured in epifluorescence images, using ImageJ. The average cell morphology values in each condition were then used to simulate TIR-FCS experiments to determine the diffusion coefficient bias[77]. The corrected diffusion coefficient was obtained by dividing the experimentally measured diffusion coefficient value by the corresponding bias value.

RNA extraction, sequencing and gene set enrichment analysis

Bacteria (10^9 cells) were harvested (5000 × *g*, 3 min) from mineral water suspensions (biological triplicates at 10^8 cells/mL) in the first day and after 7 days of incubation, and immediately flash-frozen in liquid nitrogen and stored at −80 °C until further processing. Total RNAs were recovered from bead-beaten bacterial cells using a phenol/chloroform extraction method. Purified RNA samples were further prepared for sequencing at the I2BC sequencing platform (Gif-sur-Yvette, France)

RNA sample quality was assessed in an Agilent Bioanalyzer 2100, using the RNA 6000 pico kit (Agilent Technologies, #5067-1513). Total RNAs (450 ng) were treated with Baseline-ZERO DNase (Illumina, Epicentre, #DB0715K) and ribosomal RNA was removed using the Ribo-Zero Magnetic Kit (Bacteria) (Illumina, Epicentre, #MRZB12424), according to the manufacturer recommendations. Directional RNA sequencing libraries were constructed using the TruSeq Stranded Total RNA Library Prep kit (Illumina) and sequenced (paired-end 2 × 75-bp) in a NextSeq500 instrument (Illumina). Alignment to the reference genome sequence of *Listeria monocytogenes* EGDe (RefSeq: NC_003210.1) was done using bowtie2 (v2.4.4)[78]. For the detection of differentially expressed genes (DEGs), relative library sizes, fold changes ($\log_2$FC) and p-values were estimated using the R package DESeq2 (v1.38.3)[79], and p-values were then converted to q-values using the R package fdrtool (v1.2.17)[80]. Genes with q-value ≤ 0.05 and absolute $\log_2$FC ≥ 1 were considered as DEGs.

Gene set enrichment analysis was performed on DEGs using the FUNAGE-Pro web server (http://funagepro.molgenrug.nl)[81]. A single-list analysis (gene locus tags) was done against the *Listeria monocytogenes* EGD-e reference genome (RefSeq: NC_003210.1). Gene ontology (GO) and KEGG pathway terms with a *p*-value ≤ 0.05 were considered to be statistically enriched.

Chicken embryo infection assay

The chicken embryo model was used to test the recovery of *Lm* from a VBNC state in mineral water suspensions, as previously described[50,82].

Embryonated eggs from white Leghorn chickens raised under specific pathogen-free (SPF) conditions were obtained from the Infectiology of Farm, Model and Wildlife Animals Facility (PFIE) at the INRAE Centre Val de Loire (Nouzilly, France). Intact eggs were placed in an incubator (FIEM; Guanzate, Italy) at 37.7 °C and 47% humidity, under gentle rocking motion, to initiate embryo development. After 6 days, eggs were candled to check for signs of developing embryos, such as a strong vascularized network and embryo movement. Eggs showing underdeveloped or collapsed blood vessels were discarded, while eggs with no signs of embryo development (absence of blood vessels) were set aside to be used as non-embryonated eggs. Egg shells were sterilized with 70% ethanol and perforated just above the border of the air sac to allow the injection of 100 µL of bacterial suspension into the allantoic cavity (or albumen in non-embryonated eggs), using a 25 G (0.5 × 16 mm) needle. Shell punctures were sealed with a sticky tag and the eggs were returned to the incubator. At 48 h post-inoculation, embryonated eggs were candled to discard dead embryos, and viable embryos were euthanized by incubation at 4 °C for 2 h. Embryos were recovered in aseptic conditions and placed into a tube with 4 mL of sterile DPBS to undergo mechanical homogenization (T-25 Ultra-Turrax, IKA). Serial dilutions of the embryo homogenate (or albumen from non-embryonated eggs) in DPBS were plated (500 µL) on BHI agar and incubated at 37 °C for at least 24 h to assess the presence of culturable *Lm*.

For inoculation of eggs with VBNC *Lm*, suspensions of EGDe-GFP at 10^6 bacteria/mL were prepared 28 days before, and their viability and culturability were checked to select the one with the lowest residual culturability. As a result, we used an inoculum containing 10^6 viable *Lm*/mL and 0.5 *Lm* CFU/mL, which corresponded to an inoculated dose containing 10^5 viable and 0.05 culturable bacteria. Injections of 100 µL of mineral water or a suspension of vegetative EGDe-GFP – prepared by washing and diluting bacteria from an overnight-grown culture to approximately 5000 CFU/mL—were included as negative and positive controls, respectively.

To assess whether bacterial growth recovered from inoculated eggs resulted from the revival of VBNC cells or solely from the regrowth of residual culturable bacteria, we compared the frequency of bacterial growth obtained before and after egg inoculation with the VBNC *Lm* suspension. The frequency before inoculation was determined by serially inoculating wells of a 96-well plate containing 100 µL of BHI broth with 100 µL of the VBNC *Lm* suspension, and calculating the fraction of inoculated wells showing bacterial growth after 48 h of incubation at 37 °C. Similarly, the frequency after inoculation was determined from the fraction of inoculated eggs scored positive for bacterial growth on BHI agar.

Statistics

Data obtained from experiments performed with three independent biological replicates ($n = 3$) are represented as mean ± standard deviation or median + interquartile range. Prism software (GraphPad Software, v10) was used to generate graphs and to perform statistical analyzes. Statistical tests (including correction tests for multiple comparisons) and significance values are reported in the figures and/or corresponding legends, while additional test details can be found in the Source Data file. Differences between group means were considered statistically significant for p-values ≤ 0.05.

Reporting summary

Further information on research design is available in the Nature Portfolio Reporting Summary linked to this article.

Data availability

RNA sequencing data generated in this study have been deposited in the NCBI Gene Expression Omnibus (GEO) database under the GEO Series accession number GSE246157. Source data are provided with this paper.

References

1. Beskrovnaya, P., Sexton, D. L., Golmohammadzadeh, M., Hashimi, A. & Tocheva, E. I. Structural, metabolic and evolutionary comparison of bacterial endospore and exospore formation. *Front. Microbiol.* **12**, 452 (2021).
2. Dong, K. et al. Induction, detection, formation, and resuscitation of viable but non-culturable state microorganisms. *Compr. Rev. food Sci. food Saf.* **19**, 149–183 (2020).
3. Ayrapetyan, M., Williams, T. & Oliver, J. D. Relationship between the viable but nonculturable state and antibiotic persister cells. *J. Bacteriol.* **200**, 580 (2018).
4. Li, L., Mendis, N., Trigui, H., Oliver, J. D. & Faucher, S. P. The importance of the viable but non-culturable state in human bacterial pathogens. *Front. Microbiol.* **5**, 258 (2014).
5. Baker, R. M., Singleton, F. L. & Hood, M. A. Effects of nutrient deprivation on *Vibrio cholerae*. *Appl. Environ. Microbiol.* **46**, 930–940 (1983).
6. Signoretto, C., Lleò, M. D. M. & Canepari, P. Modification of the peptidoglycan of *Escherichia coli* in the viable but nonculturable state. *Curr. Microbiol.* **44**, 125–131 (2002).
7. Signoretto, C., Lleò, M. D. M., Tafi, M. C. & Canepari, P. Cell wall chemical composition of *Enterococcus faecalis* in the viable but nonculturable state. *Appl. Environ. Microbiol.* **66**, 1953–1959 (2000).
8. Costa, K. et al. The morphological transition of *Helicobacter pylori* cells from spiral to coccoid is preceded by a substantial modification of the cell wall. *J. Bacteriol.* **181**, 3710–3715 (1999).
9. Errington, J., Mickiewicz, K., Kawai, Y. & Wu, L. J. L-form bacteria, chronic diseases and the origins of life. *Philos. Trans. R. Soc. B Biol. Sci.* **371**, 20150494 (2016).
10. Wohlfarth, J. C. et al. L-form conversion in Gram-positive bacteria enables escape from phage infection. *Nat. Microbiol.* **8**, 387–399 (2023).
11. Kawai, Y., Mickiewicz, K. & Errington, J. Lysozyme counteracts β-lactam antibiotics by promoting the emergence of L-form bacteria. *Cell* **172**, 1038–1049.e10 (2018).
12. Besnard, V., Federighi, M. & Cappelier, J. M. Evidence of viable but non-culturable state in *Listeria monocytogenes* by direct viable count and CTC-DAPI double staining. *Food Microbiol.* **17**, 697–704 (2000).
13. Besnard, V., Federighi, M., Declerq, E., Jugiau, F. & Cappelier, J. M. Environmental and physico-chemical factors induce VBNC state in *Listeria monocytogenes*. *Vet. Res.* **33**, 359–370 (2002).
14. Wideman, N. E., Oliver, J. D., Crandall, P. G. & Jarvis, N. A. Detection and potential virulence of viable but non-culturable (VBNC) *Listeria monocytogenes*: a review. *Microorganisms* **9**, 1–11 (2021).
15. Stiefel, P., Schmidt-Emrich, S., Maniura-Weber, K. & Ren, Q. Critical aspects of using bacterial cell viability assays with the fluorophores SYTO9 and propidium iodide. *BMC Microbiol.* **15**, 36 (2015).
16. Domínguez-Cuevas, P., Mercier, R., Leaver, M., Kawai, Y. & Errington, J. The rod to L-form transition of *Bacillus subtilis* is limited by a requirement for the protoplast to escape from the cell wall sacculus. *Mol. Microbiol.* **83**, 52–66 (2012).
17. Dell'Era, S. et al. *Listeria monocytogenes* L-forms respond to cell wall deficiency by modifying gene expression and the mode of division. *Mol. Microbiol.* **73**, 306–322 (2009).
18. Fiedler, F. Biochemistry of the cell surface of *Listeria* strains: a locating general view. *Infection* **16**, S92–S97 (1988).
19. Bishop, D. K. & Hinrichs, D. J. Adoptive transfer of immunity to *Listeria monocytogenes*. The influence of in vitro stimulation on lymphocyte subset requirements. *J. Immunol.* **139**, 2005–2009 (1987).
20. Jonquières, R., Bierne, H., Mengaud, J. & Cossart, P. The *inlA* gene of *Listeria monocytogenes* LO28 harbors a nonsense mutation resulting in release of internalin. *Infect. Immun.* **66**, 3420–3422 (1998).
21. Aguilar-Bultet, L. et al. Genetic separation of *Listeria monocytogenes* causing central nervous system infections in animals. *Front. Cell. Infect. Microbiol.* **8**, 20 (2018).

22. Rismondo, J., Haddad, T. F. M., Shen, Y., Loessner, M. J. & Gründling, A. GtcA is required for LTA glycosylation in *Listeria monocytogenes* serovar 1/2a and Bacillus subtilis. *Cell Surf* **6**, 100038 (2020).
23. Shen, Y. et al. Structural and functional diversity in *Listeria* cell wall teichoic acids. *J. Biol. Chem.* **292**, 17832–17844 (2017).
24. Schardt, J. et al. Comparison between *Listeria sensu stricto* and *Listeria sensu lato* strains identifies novel determinants involved in infection. *Sci. Rep.* **7**, 17821 (2017).
25. Yoon, Y., Lee, H., Lee, S., Kim, S. & Choi, K.-H. Membrane fluidity-related adaptive response mechanisms of foodborne bacterial pathogens under environmental stresses. *Food Res. Int.* **72**, 25–36 (2015).
26. Scheinpflug, K., Krylova, O. & Strahl, H. Measurement of cell membrane fluidity by Laurdan GP: fluorescence spectroscopy and microscopy. *Methods Mol. Biol.* **1520**, 159–174 (2017).
27. Barbotin, A., Billaudeau, C., Sezgin, E. & Carballido-López, R. Quantification of membrane fluidity in bacteria using TIR-FCS. *Biophys. J.* https://doi.org/10.1016/j.bpj.2024.06.012 (2024).
28. Cunningham, E., O'Byrne, C. & Oliver, J. D. Effect of weak acids on *Listeria monocytogenes* survival: Evidence for a viable but non-culturable state in response to low pH. *Food Control* **20**, 1141–1144 (2009).
29. Robben, C. et al. Induction of the viable but non-culturable state in bacterial pathogens by household cleaners and inorganic salts. *Sci. Rep.* **8**, 15132 (2018).
30. Highmore, C. J., Warner, J. C., Rothwell, S. D., Wilks, S. A. & Keevil, C. W. Viable-but-nonculturable *Listeria monocytogenes* and *Salmonella enterica* Serovar Thompson induced by chlorine stress remain infectious. *MBio* **9**, e00540–18 (2018).
31. Noll, M. et al. Benzalkonium chloride induces a VBNC state in *Listeria monocytogenes*. *Microorganisms* **8**, 184 (2020).
32. Lindbäck, T., Rottenberg, M. E., Roche, S. M. & Rørvik, L. M. The ability to enter into an avirulent viable but non-culturable (VBNC) form is widespread among *Listeria monocytogenes* isolates from salmon, patients and environment. *Vet. Res.* **41**, 8 (2010).
33. Bremer, P. J., Osborne, C. M., Kemp, R. A. & Smith, J. J. Survival of *Listeria monocytogenes* in sea water and effect of exposure on thermal resistance. *J. Appl. Microbiol.* **85**, 545–553 (1998).
34. Wang, X. et al. Cryptic prophages help bacteria cope with adverse environments. *Nat. Commun.* **1**, 147 (2010).
35. Ivy, R. A., Wiedmann, M. & Boor, K. J. *Listeria monocytogenes* grown at 7 °C shows reduced acid survival and an altered transcriptional response to acid shock compared to *L. monocytogenes* grown at 37 °C. *Appl. Environ. Microbiol.* **78**, 3824–3836 (2012).
36. Duru, I. C. et al. High-pressure processing-induced transcriptome response during recovery of *Listeria monocytogenes*. *BMC Genomics* **22**, 1–20 (2021).
37. Argov, T. et al. Coordination of cohabiting phage elements supports bacteria–phage cooperation. *Nat. Commun.* **10**, 1–14 (2019).
38. Irving, S. E., Choudhury, N. R. & Corrigan, R. M. The stringent response and physiological roles of (pp)pGpp in bacteria. *Nat. Rev. Microbiol.* **19**, 256–271 (2021).
39. Bai, K. et al. The role of RelA and SpoT on ppGpp production, stress response, growth regulation, and pathogenicity in *Xanthomonas campestris* pv. *campestris*. *Microbiol. Spectr.* **9**, e0205721 (2021).
40. Boaretti, M., Lleò, M. D. M., Bonato, B., Signoretto, C. & Canepari, P. Involvement of *rpoS* in the survival of *Escherichia coli* in the viable but non-culturable state. *Environ. Microbiol.* **5**, 986–996 (2003).
41. Whiteley, A. T., Pollock, A. J. & Portnoy, D. A. The PAMP c-di-AMP is essential for *Listeria monocytogenes* growth in rich but not minimal media due to a toxic increase in (p)ppGpp. [corrected]. *Cell Host Microbe* **17**, 788–798 (2015).
42. Höltje, J.-V. V. Growth of the stress-bearing and shape-maintaining murein sacculus of *Escherichia coli*. *Microbiol. Mol. Biol. Rev.* **62**, 181–203 (1998).
43. Bierne, H. & Cossart, P. *Listeria monocytogenes* surface proteins: from genome predictions to function. *Microbiol. Mol. Biol. Rev.* **71**, 377–397 (2007).
44. Popowska, M. & Markiewicz, Z. Characterization of *Listeria monocytogenes* protein Lmo0327 with murein hydrolase activity. *Arch. Microbiol.* **186**, 69–86 (2006).
45. Pinto, D., São-José, C., Santos, M. A. & Chambel, L. Characterization of two resuscitation promoting factors of *Listeria monocytogenes*. *Microbiol. (United Kingdom)* **159**, 1390–1401 (2013).
46. Carroll, S. A. et al. Identification and characterization of a peptidoglycan hydrolase, MurA, of *Listeria monocytogenes*, a muramidase needed for cell separation. *J. Bacteriol.* **185**, 6801–6808 (2003).
47. Lenz, L. L., Mohammadi, S., Geissler, A. & Portnoy, D. A. SecA2-dependent secretion of autolytic enzymes promotes *Listeria monocytogenes* pathogenesis. *Proc. Natl. Acad. Sci. USA.* **100**, 12432–12437 (2003).
48. Machata, S., Hain, T., Rohde, M. & Chakraborty, T. Simultaneous deficiency of both MurA and p60 proteins generates a rough phenotype in *Listeria monocytogenes*. *J. Bacteriol.* **187**, 8385–8394 (2005).
49. Lotoux, A., Milohanic, E. & Bierne, H. The viable but non-culturable state of *Listeria monocytogenes* in the One-Health Continuum. *Front. Cell. Infect. Microbiol.* **12**, 849915 (2022).
50. Cappelier, J. M., Besnard, V., Roche, S. M., Velge, P. & Federighi, M. Avirulent viable but non culturable cells of *Listeria monocytogenes* need the presence of an embryo to be recovered in egg yolk and regain virulence after recovery. *Vet. Res.* **38**, 573–583 (2007).
51. Cappelier, J. M., Minet, J., Magras, C., Colwell, R. R. & Federighi, M. Recovery in embryonated eggs of viable but nonculturable *Campylobacter jejuni* cells and maintenance of ability to adhere to HeLa cells after resuscitation. *Appl. Environ. Microbiol.* **65**, 5154–5157 (1999).
52. Chaveerach, P., ter Huurne, A. A. H. M., Lipman, L. J. A. & van Knapen, F. Survival and resuscitation of ten strains of *Campylobacter jejuni* and *Campylobacter coli* under acid conditions. *Appl. Environ. Microbiol.* **69**, 711–714 (2003).
53. Talibart, R., Denis, M., Castillo, A., Cappelier, J. M. & Ermel, G. Survival and recovery of viable but noncultivable forms of *Campylobacter* in aqueous microcosm. *Int. J. Food Microbiol.* **55**, 263–267 (2000).
54. Besnard, V., Federighi, M. & Cappelier, J. M. Development of a direct viable count procedure for the investigation of VBNC state in *Listeria monocytogenes*. *Lett. Appl. Microbiol.* **31**, 77–81 (2000).
55. Gião, M. S. & Keevil, C. W. *Listeria monocytogenes* can form biofilms in tap water and enter into the viable but non-cultivable state. *Microb. Ecol.* **67**, 603–611 (2014).
56. Dreux, N. et al. Viable but non-culturable *Listeria monocytogenes* on parsley leaves and absence of recovery to a culturable state. *J. Appl. Microbiol.* **103**, 1272–1281 (2007).
57. Cappelier, J. M. et al. Avirulence of viable but non-culturable *Listeria monocytogenes* cells demonstrated by in vitro and in vivo models. *Vet. Res.* **36**, 589–599 (2005).
58. Ramijan, K. et al. Stress-induced formation of cell wall-deficient cells in filamentous actinomycetes. *Nat. Commun.* **9**, 1–13 (2018).
59. Claessen, D. & Errington, J. Cell wall deficiency as a coping strategy for stress. *Trends Microbiol.* **27**, 1025–1033 (2019).
60. Parry, B. R. et al. The bacterial cytoplasm has glass-like properties and is fluidized by metabolic activity. *Cell* **156**, 183–194 (2014).
61. Weller, D., Wiedmann, M. & Strawn, L. K. Irrigation is significantly associated with an increased prevalence of *Listeria monocytogenes* in produce production environments in New York State. *J. Food Prot.* **78**, 1132–1141 (2015).
62. Sharma, M. et al. Prevalence of *Salmonella* and *Listeria monocytogenes* in non-traditional irrigation waters in the Mid-Atlantic

United States is affected by water type, season, and recovery method. *PLoS One* **15**, e0229365 (2020).
63. Lyautey, E. et al. Distribution and characteristics of *Listeria monocytogenes* isolates from surface waters of the South Nation River watershed, Ontario, Canada. *Appl. Environ. Microbiol.* **73**, 5401–5410 (2007).
64. Raschle, S. et al. Environmental dissemination of pathogenic *Listeria monocytogenes* in flowing surface waters in Switzerland. *Sci. Rep.* **11**, 9066 (2021).
65. Bécavin, C. et al. Listeriomics: an Interactive Web Platform for Systems Biology of *Listeria*. *mSystems* **2**, https://doi.org/10.1128/msystems.00186-16 (2017).
66. Zhao, X., Zhong, J., Wei, C., Lin, C.-W. & Ding, T. Current perspectives on viable but non-culturable state in foodborne pathogens. *Front. Microbiol.* **8**, 580 (2017).
67. Slavchev, G., Michailova, L. & Markova, N. Stress-induced L-forms of *Mycobacterium bovis*: a challenge to survivability. *New Microbiol.* **36**, 157–166 (2013).
68. Dannenberg, N. et al. Mycobacteria form viable cell wall-deficient cells that are undetectable by conventional diagnostics. *bioRxiv* 2022.11.16.516772 https://doi.org/10.1101/2022.11.16.516772 (2022).
69. Monk, I. R., Gahan, C. G. M. & Hill, C. Tools for functional post-genomic analysis of *Listeria monocytogenes*. *Appl. Environ. Microbiol.* **74**, 3921–3934 (2008).
70. Lauer, P., Chow, M. Y. N., Loessner, M. J., Portnoy, D. A. & Calendar, R. Construction, characterization, and use of two *Listeria monocytogenes* site-specific phage integration vectors. *J. Bacteriol.* **184**, 4177–4186 (2002).
71. Sun, L. et al. AsnB Mediates Amidation of Meso-Diaminopimelic Acid Residues in the Peptidoglycan of *Listeria monocytogenes* and Affects Bacterial Surface Properties and Host Cell Invasion. *Front. Microbiol.* **12**, 760253 (2021).
72. Schindelin, J. et al. Fiji: an open-source platform for biological-image analysis. *Nat. Methods* **9**, 676–682 (2012).
73. Mastronarde, D. N. SerialEM: a program for automated tilt series acquisition on Tecnai microscopes using prediction of specimen position. *Microsc. Microanal.* **9**, 1182–1183 (2003).
74. Mastronarde, D. N. & Held, S. R. Automated tilt series alignment and tomographic reconstruction in IMOD. *J. Struct. Biol.* **197**, 102–113 (2017).
75. Pettersen, E. F. et al. UCSF ChimeraX: structure visualization for researchers, educators, and developers. *Protein Sci.* **30**, 70–82 (2021).
76. Touche, C., Hamchaoui, S., Quilleré, A., Darsonval, M. & Dubois-Brissonnet, F. Growth of *Listeria monocytogenes* is promoted at low temperature when exogenous unsaturated fatty acids are incorporated in its membrane. *Food Microbiol.* **110**, 104170 (2023).
77. Barbotin, A., Billaudeau, C., Sezgin, E. & LOPEZ, R. C. Quantification of membrane fluidity in bacteria using TIR-FCS. *bioRxiv* 2023.10.13.562271 https://doi.org/10.1101/2023.10.13.562271 (2023).
78. Langmead, B. & Salzberg, S. L. Fast gapped-read alignment with Bowtie 2. *Nat. Methods* **9**, 357–359 (2012).
79. Love, M. I., Huber, W. & Anders, S. Moderated estimation of fold change and dispersion for RNA-seq data with DESeq2. *Genome Biol.* **15**, 550 (2014).
80. Strimmer, K. fdrtool: A versatile R package for estimating local and tail area-based false discovery rates. *Bioinformatics* **24**, 1461–1462 (2008).
81. de Jong, A., Kuipers, O. P. & Kok, J. FUNAGE-Pro: comprehensive web server for gene set enrichment analysis of prokaryotes. *Nucleic Acids Res.* **50**, W330–W336 (2022).
82. Andersson, C., Gripenland, J. & Johansson, J. Using the chicken embryo to assess virulence of *Listeria monocytogenes* and to model other microbial infections. *Nat. Protoc.* **10**, 1155–1164 (2015).

Acknowledgements

We dedicate this work to the memory of Hélène Bierne and Fabrizia Stavru. We thank Didier Cabanes (U. Porto, Portugal), Daniel Portnoy (UC Berkeley, California, USA) and Anna Oevermann (U. Bern, Switzerland), for gifting us *Listeria* strains, and Jasmina Vidic, for help with the laurdan GP assays. We acknowledge the sequencing and bioinformatics expertize of the I2BC high-throughput sequencing facility, supported by France Génomique (funded by the French government's Programme Investissements d'Avenir (PIA): ANR-10-INBS-0009). We acknowledge the cryo-ET expertize and assistance of the Institut Pasteur NanoImaging Core facility, created and supported by a PIA grant (EquipEx CACSICE: ANR-11-EQPX-0008). We thank the members of the EpiMic team for helpful discussions, and Simonetta Gribaldo, Delphine Lechardeur, Philippe Noirot and Pascale Cossart, for critical feedback to this manuscript. This work was supported by grants from the Agence Nationale de la Recherche (ANR) to H.B. (PERMALI: ANR-20-CE35-0001-01) and A.P. (THOR: ANR-20-CE15-0008-01); from the Université Paris-Saclay to H.B. (DEPISTALIS, AAP Poc in labs 2019); from INRAE's MICA department and Micalis Institute to A.P. (AAP Micalis 2023); and from the European Research Council, under the Horizon 2020 research and innovation program, to R.C.L. (agreement ID: 772178). F.C. was supported by postdoctoral grants from INRAE MICA department. A.B. was supported by the EU Horizon 2020 research and innovation program, under the Marie Skłodowska-Curie Actions grant (agreement ID: 101030628).

Author contributions

F.C., H.B. and A.P. conceived the research plan and methodology. E.M. conceived and performed pilot experiments. F.C., A.C., A.S.R., S.T., A.D.G., P.C., P.N., F.D.B., A.B., E.D., M.B., K.G., C.S., M.P.C.C., E.M. and A.P. performed experiments. F.C., A.S.R., A.D.G., P.N., F.D.B. and A.B. analyzed collected data. A.S.R., S.T., P.N., F.D.B., K.G., R.C.L., M.P.C.C., H.B. and A.P. provided resources (reagents, equipment, analysis tools). F.C., H.B. and A.P. wrote the original manuscript. F.C., E.M., H.B. and A.P. reviewed and edited the manuscript. F.C. prepared and organized data visualization. H.B. and A.P. provided funding and supervision. All authors contributed to this work and approved the submitted version.

Competing interests

The authors declare no competing interests.

Additional information

Supplementary information The online version contains supplementary material available at https://doi.org/10.1038/s41467-024-52633-7.

Correspondence and requests for materials should be addressed to Alessandro Pagliuso.

Peer review information *Nature Communications* thanks William Nicolas, Stephan Schmitz-Esser and the other, anonymous, reviewer(s) for their contribution to the peer review of this work. A peer review file is available.